Development of Polymer Coated Nanoparticles and Polymer Bridged Magnetic Luminescent Hybrids

by

Hande Öztürk

A Thesis Submitted to the

Graduate School of Engineering

in Partial Fulfillment of the Requirements for

the Degree of

Master of Science

in

Materials Science and Engineering

Koc University

September 2010

Koc University

Graduate School of Sciences and Engineering

This is to certify that I have examined this copy of a master's thesis by

Hande Öztürk

and have found that it is complete and satisfactory in all respects,

and that any and all revisions required by the final

examining committee have been made.

Committee Members:

_____

H.Funda Yağcı Acar, Ph. D. (Advisor)

_____

Ersin Acar, Ph. D.

_____

Uğur Ünal, Ph. D.

Date: _____

Abstract

Nanoparticles have been a center of focus in both academic and industrial research due to their unique properties. In particular, quantum dots and superparamagnetic iron oxide have been studied extensively, as elements in a wide range of technologies. With the advances in control over synthesis and properties, a desire to incorporate multiple functions in a single hybrid nanoparticle has developed in the recent years. Hybrid nanoparticles created an excitement in areas such as sensors, biotechnology, medicine, solar cells.

Quantum dots (QD) with size tunable properties and long luminescence lifetimes and superparamagnetic iron oxides (SPIO) with biocompatible and response to magnetic field have been two of the most studied nanoparticles in the nano-biotechnology. Combining these two particles in a single entity would be extremely useful in a wide range of application but mostly for the multiplicity in sensors, labeling and in medicine/biotechnology where dual imaging and dual action of sensing and separation, imaging and therapy, labeling and delivery can be obtained.

In realization of such hybrid nanoparticles, a novel approach was designed: Magnetic luminescent nanoparticles from CdS and SPIO were developed using block copolymers. First of all, surface initiated polymerization (ATRP) was performed and PS-b-PHEMA and PS-b-PDMAEMA were grown from the surface of SPIO.

Secondly, CdS quantum dots were synthesized in the presence of the PDMAEMA that will be used to connect two nanoparticle. For the first time in literature, a detailed investigation was conducted on the synthesis and stimuli responsive behavior of PDMAEMA coated CdS nanoparticles. This part of study is not only a major step towards the synthesis of our final hybrid structure, but also an extensive subject of study in itself.

Finally, first example of magnetic/luminescent nanoparticles connected via amphiphilic block copolymers was demonstrated. The full characterization of the final structure is still ongoing.

Development of smart magnetic/luminescent hybrid structure creates an exciting opportunity for multifunctional materials that would impact the fields of biological labeling, medical imaging, sensing and separation with an advantage of multiplexing and combined action of dual sensing and separation.

Özet

Nanoparçacıklar (NP) son birkaç on yılda sahip oldukları eşsiz özellikler nedeniyle hem endüstriyel hem de akademik araştırmaların odağında yer almışlardır. Kuantum noktacıkları ve süperparamanyetik demir oksit nanoparçacıkları çok çeşitli sahalarda çalışılmıştır. Özellikle sensör, medikal görüntüleme, güneş pilleri gibi uygulama sahalarında farklı nanoparçacıklardan oluşan hibrid malzemeler ilgi çekmeye başlamıştır. Nanoparçacıkların sentezi ve özelliklerini kontrol etmedeki başarı son yıllarda birden çok fonksiyonu bir arada taşıyan hibrid nanoparçacıklara heves ve ihtiyacı kamçılamıştır. Bu tür hybrid parçacıklar pek çok sahada ama öncelikle sensör, biyoteknoloji, tıp ve enerji sahasında ilgi çekmektedir

Kuantum noktacıkları (KN) büyüklüğe bağlı optik özellikleri ve uzun ışıma süreleri, süperparamanyetik demir oksitler (SDO) ise biyouyumluluğu ve manyetik sahaya yanıt vermeleri nedeniyle nano-biyoteknoloji sahasında en çok çalışılan nanoparçacıklar olmuşlardır. Bu iki parçacığın bir arada bulunduğu hibrid yapılar pek çok uygulama alanı için önemlidir ama özellikle sensör ve etiketleme sahasında çokluk, medikal sahada ikili görüntüleme ve görüntüleme-terapi, yönlendirme-görüntüleme gibi kombine aksiyonları bir arada yapabilme olanaklarını sağlayacak çok kıymetli ve ilgi çekici malzemelerdir.

Bu hibrid nanoparçacıkların sentezinde yeni bir yaklaşım geliştirildi ve CdS ve SDO nanoparçacıkları blok polimerler vasıtasıyla bir araya getirildi. İlk olarak, PS-b-PHEMA ve PS-b-PDMAEMA polimerleri ,yüzeyinden kontrollü polimerleşme (ATRP) metoduyla SDO yüzeyinden büyütüldüler.

İkinci olarak, CdS kuantum noktacıkları, daha sonra iki nanoparçacığı bağlayacak köprü görevini görecek PDMAEMA varlığında sentezlendiler. Literatürde ilk defa, PDMAEMA kaplı CdS nanoparçacıklarının sentezi ve sensör özellikleri detaylı bir şekilde incelendi. Çalışmanın bu kısmı sadece hedeflenen hibrid yapısına ulaşmakta önemli bir adım olmakla kalmayıp, başlı başına ayrı bir araştırma konusu niteliğindedir.

Son olarak, amfifilik blok kopolimerlerle bağlanmış ışıyan/manyetik hibrid nanoparçacıkların ilk örneği sentezlenmiştir.Nihai yapının karakterizasyonu halen devam etmektedir.

Akıllı ışıyan/manytik hibrid yapıların geliştirilmesi, çifte algılama ve ayırmanın çoklayıcı ve birleştirici avantajları sayesinde, biyolojik etiketleme, tıbbi görüntüleme, algı ve ayırma alanlarında çokişlevli malzemeler için heyecan verici bir fırsat yaratmaktadır.

Acknowledgements

I would like to express my deep appreciation and thanks for my advisor. With infinite patience, she guided me through the work I am proud to present

Table of Contents

Index of Figures

Index of Tables

Abbreviations

AC	Alternating Current
APTMS	3-Aminopropyltriethoxysilane
ATRP	Atom Transfer Radical Polymerization
BPTMS	2-Bromo propionamide propyltrimethoxysilane
BSA	Bovine Serum Albumin
CPTMS	Chloromethylphenyl trimethoxysilane
DLS	Dynamic Light Scattering
DMF	Dimethylformamide
DNA	Deoxyribo Nucleic Acid
EBIB	Ethyl 2-Bromoisobutyrate
FTIR	Fourier Transformed Infra-Red
GPC	Gel Permeation Chromothography
HEMA	(Hydroxyethyl)methacrylate
HMTETA	Hexamethyltriethylenetetraamine
HOMO	Highest Occupied Molecular Orbital
IPA	Isopropanol
KN	Kuantum Noktası
LA	Lauric Acid
LCST	Lower critical solution temperature
LUMO	Lowest Unoccupied Molecular Orbital
MA	Methyl Acrylate
Me-TREN	Tris [2-(dimetylamino) ethyl]amine
MMA	Methyl Methacrylate
MNP	Magnetic Nanoparticle
MW	Molecular Weight
NP	Nanoparçacık

o-DCB	o-Dichlorobenzene
PAA	Poly(acrylic acid)
PDMAEMA	Poly(dimethylaminoethylmethacrylate)
PDI	Polydispersity Index
PHEMA	Poly((hydroxyethyl)methacrylate)
PMDETA	Pentamethyldiethylenetriamine
PMMA	Poly(methyl methacrylate)
PS	Poly(styrene)
PS-b-PDMAEMA	Poly(styrene)-b-Poly(dimethylaminoethylmethacrylate)
PS-b-PHEMA	Poly(styrene)-b-Poly((hydroxyethyl)methacrylate)
QD	Quantum Dot
QY	Quantum Yield
RAFT	Reversible Addition-Fragmentation chain Transfer
ROMP	Ring opening metathesis polymerization
SDO	Süperparamanyetik Demir Oksit
SDS	Sodium Dodecylsulfate
SI-ATRP	Surface Initiated Atom Transfer Radical Polymerization
SIP	Surface Initiated Polymerization
SPIO	Superparamagnetic Iron oxide
TEA	Triethylamine
TGA	Thermo Gravimetric Analysis
THF	Tetrahydrofuran
TMEDA	Tetramethylethylenediamine
TOPO	Trioctylphosphine Oxide

Chapter 1 INTRODUCTION

Over the past few decades, distinct chemical, physical and biological properties made nanoparticles focus of attention. Nanoparticles of a wide variety of composition, such as gold, silver, carbon, semiconductors, silicon and metal oxides, and a variety of shapes, including nanospheres, nanotubes, and nanocages, have been developed with unique properties and found use in fields of chemistry, material sciences, physics, medicine and electronics [1-3]. In terms of magnetic, photonic, chemical and electrical properties, nanoparticles exhibit dramatically different behavior, compared to their bulk counterparts, due to their size confinement. As an example, gold and silver nanoparticles absorb the visible light at a definite wavelength and emit it back at another, both of which can be tuned by the size and the shape of the nanoparticles [4].

Quantum dots and iron oxides, along with silica nanoparticles and gold, make up the most studied types of nanoparticles. Quantum dots and superparamagnetic iron oxide nanoparticles are the subjects of this thesis. Due to quantum confinement and surface effects, quantum dots possess size-tunable optical properties. Consequently, they are frequently employed as fluorescent tags in biology and in photonic applications [5-6].

Another unique property observed at nanoscale and exploited in nanoparticles, especially iron oxide nanoparticles, is superparamagnetism, where a particle exhibits magnetism only under the influence of a magnetic field. These materials are paramagnetic even below the Curie temperature. Generally, these are single domain, single crystal nanoparticles of 10 nm or less. In paramagnetic materials where spin alignment happens in domains, in superparamagnetic materials, the magnetic moment of the entire crystallite tends to align with the magnetic field creating a higher saturation value. Iron oxide nanoparticles, magnetite (Fe_3O_4) and maghemite (Fe_2O_3), show superparamagnetic behavior at room temperature, are biocompatible and biodegradable, so are widely studied. Magnetite, which is black, has a magnetic saturation of 92-100 J/T.kg at 300 K. Maghemite, on the other hand, has a bit lower magnetic saturation (60-80 J/T.kg) and is dark brown [7]. Superparamagnetic iron

oxides (SPIOs) are frequently exploited in sensors, magnetic separation, therapy, medical imaging, audio speakers, seals, etc. [8].

Other than controlling the size, functionalization of the nanoparticle surface is a very important and a very complex issue. Surface functionalization is usually achieved through the coating of nanocrystal. Coating has to satisfy a number of criterions. First of all, it has to stabilize nanoparticles in solution. During the growth it should control the growth, size and the shape of resulting particles. Chemistry of the coating should be suitable for the targeted tasks. The coating is the part of the nanoparticle which interacts with the carrier solvent or the medium/material that nanoparticles will interact with. Therefore, the coating should be compatible with the carrier medium. Usually, coatings with reactive functional groups at the outer surface, to provide a basis for further derivatization, are desired. Furthermore, coated nanoparticle, the assembly in another word, should be stable enough to endure processing and environmental forces, such as oxidation, to prevent premature deactivation or aggregation. Finally, especially for medical applications, the resulting nanoparticle should be non-toxic and biocompatible.

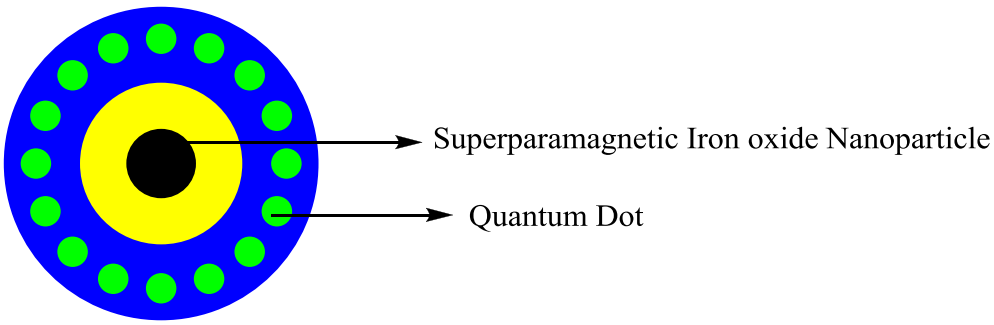

Figure 1. Multifunctional nanoparticle: all in one

Much effort has been made to define strategies for surface functionalization of superparamagnetic iron oxide nanoparticles (SPIOs) to satisfy these criteria. These nanoparticles are generally formed in a core-shell structure where the magnetic core is surrounded by a coating that adsorbs on the crystal surface and is suitable for the desired application. A variety of small molecules with silane, carboxylic acid and alcohol functional groups has been successfully adopted as coatings for iron oxide

nanoparticles [9, 10]. These coating materials not only determine the solubility or miscibility but also used to prevent aggregation and provide colloidal stability by altering the interparticle interactions. Particles experience repulsive and attractive forces as they approach one another in the solution. Stability of a colloidal system is the sum of these forces. Repulsive forces consist of electrostatic repulsion, which is a result of charged species in the system and steric repulsion caused by the coatings adsorbed onto the particle. These forces cause an energy barrier, which prevents two particles to come close to one another and stick together. If the particles come together and be able to pass this energy barrier, then attractive force, which is a result of Van der Waals interaction, causes the particles to adhere each other. In magnetic nanoparticles, magnetic interactions can cause aggregation as well.

Adsorption of the surfactants on growing crystal is effective in controlling the particle size, as well. Yet, the binding strength is a key issue when stability is a concern for the application. Carboxylic acid containing species are proven as effective coatings for iron oxide through chemical adsorption of the carboxylate on the iron oxide surface [11]. Alkoxysilanes are also successful coatings forming Fe-O-Si covalent bond, which again serves to prevent aggregation [12]. Later provides a much stronger binding compared to the former. Polymers can also be used for the coating of magnetic cores as well. Dextran, polyvinyl alcohol and polyacrylic acid are some of the major polymeric materials used with iron oxides. There are two techniques for coating the nanoparticles with polymers. One of them is '*grafting-to*' technique in which the functionalized polymers are preformed and then grafted onto the nanoparticle through physisorption or chemisorption [13]. This technique has the disadvantage of low degrees of grafting because of steric hindrance. The other and more controlled technique is called '*grafting-from*' in which well-defined polymers can functionalize the surfaces of nanoparticles by surface initiated polymerization (SIP) [14]. As a result, polymer brushes or hairy nanoparticles are formed. This does not only provide steric stabilization but also enhanced compatibility to similar polymer matrices if desired.

1.1 Quantum Dots

Quantum dots are nanometer (10^{-9} meter) scale particles that are neither small molecules, nor bulk solids. Their composition and small size, which may vary from a few hundred to a few thousand atoms, give these dots extraordinary optical properties that can be tuned by changing the size or composition of the dots. Quantum dots first absorb, and then emit light, possibly in a different color. This property, called fluoresence**,** is also found in other organic and inorganic materials. However, the ideal fluorophore is expected to be bright, non-photobleaching with narrow, symmetric emission spectra, and to have multiple resolvable colors that can be excited simultaneously using a single excitation wavelength. Quantum dots possess all of these qualities [15].

The underlying mechanism at the molecular level depends on the band gap between conduction band and valence band. The process involved is analogous to the lowest energy electronic transition, where an electron in the highest occupied molecular orbital (HOMO) is transferred to the lowest unoccupied molecular orbital (LUMO) as a result of excitation. Here, HOMO creates the electron filled valence band, while LUMO creates empty conduction band.

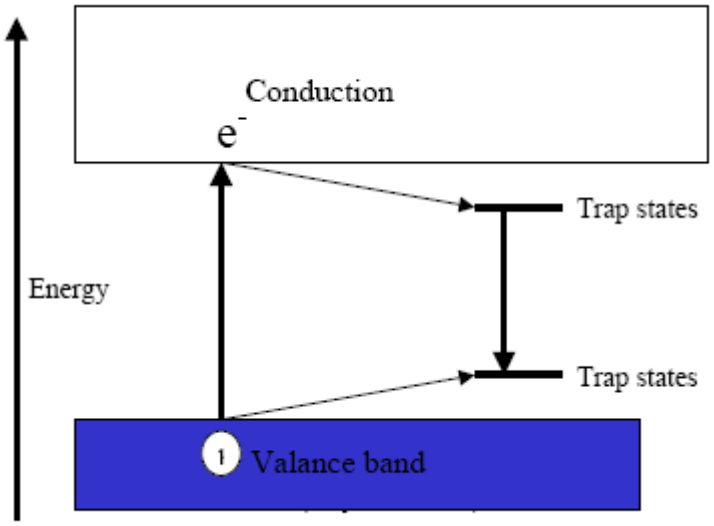

Figure 2. Simplified photoluminescence mechanism of a semiconductor [16]

For this jump to occur, the electron must attain a minimum energy, E_g band-gap energy. The resulting electron-hole pair is called an exciton. It is possible for the exciton to recombine immediately, emitting the energy equal to Eg in heat or light form. However, it is more likely for trap states within the material to catch the electron or the hole, as shown in Figure 2.

The trap states within the material arise from various sources, including structural defects, atomic vacancies, dangling bonds, and adsorbents at the interface. Radiative recombination of the trapped charge carriers then produces luminescence that is substantially red-shifted from the absorbed light. These trap states are strictly controlled by the size and surface structure of the semiconductor, hence the size controlled luminescence of quantum dots.

A very unique property of semiconductor quantum dots is the size dependence of luminescence emission. Control over both absorption and emission color, achieved by simply changing the size, is one of these properties that render quantum dots superior to its alternatives. As mentioned, surface to volume ratio has a great effect on trap states of which the mechanism is not quite clear. As the size gets smaller the band gap becomes larger. Exploiting this feature, it is possible to span the color spectrum, from infrared to ultraviolet, by using only a small amount of semiconductor material at differently sized clusters [17]. This extraordinary feature is the result of quantum confinement effect, obtained when the size of quantum dots gets smaller than their Bohr Radius, separation between the electron and the hole. Their unique chemical and electronic properties provide a potential use in the fields of nonlinear optics, luminescence, electronics, catalysis, solar energy conversion, and optoeletronics, as well as biological sensing and labeling.

1.1.1 Brus Equation and Crystal Size Determination

The Bohr model can be used to calculate the energy difference between the electron and the hole pair. The simple formula is,

$$r = \frac{\varepsilon h^2}{\pi m_r e^2} \quad (1)$$

Where r is the radius of the sphere; ε is the dielectric constant of the semiconductor; h is Plank's constant, e is the electronic charge, and m_r is the reduced mass of the electron-hole pair.

As the size of the semiconductor approaches to the Bohr radius (0.59 Å), the semiconductor shows the quantum confinement effects. The particles with 1-100Å diameter usually exhibits quantum confinement effect and are referred to as "quantum dots". Since these nanocrystals are much smaller than the wavelength of the visible light, dispersions of these materials are almost transparent. Such an effect has been observed by Chester Berry at Kodak in the absorbance spectra of AgI colloids. They attributed this phenomenon to the quantum confinement effect. The experimental work of Berry was the basis of this hypothesis [18]. Brus and Rossetti noticed that CdS nanocrystals grown in glass shows unusually blue-shift in the absorbance spectra [19]. The following formula given by Brus is very useful to make correlation between the absorption edge and the size of the particles.

$$\Delta E(d) = \frac{h^2\pi}{d^2}\left[\frac{1}{m_e^*} + \frac{1}{m_h^*}\right] - \frac{3.572e^2}{\varepsilon d} - \frac{0.24e^4\pi^2}{h^2\varepsilon^2}\left[\frac{1}{m_e^*} + \frac{1}{m_h^*}\right]^{-1} \quad (2)$$

Where ΔE(d*)* is the ground state energy of the semiconductor, *h* is Planck's constant, e is the electronic charge, *d* is the particle diameter, ε is the dielectric constant, and m_e^* and m_h^* are the effective masses of the electron and hole, respectively [20]. The first term in this equation denotes the kinetic energy of the electron and the hole, which increases with decreasing particle size which is analogous to the particle-in-a-box model. The second term represents the Coulombic stabilization of the exciton. The third term correlates the electron and the hole.

The difference in band gap energies of the bulk and confined materials is given by [19].

$$E(d) = E(bulk) \cdot \Delta E_c(d) \quad (3)$$

By using the effective mass model of Brus [21]

$$E^0(d) = E^0(bulk) \cdot \frac{h^2 \pi}{d^2 m_e^*} \quad (4)$$

1.1.2 Application of Quantum Dots

The potential applications of semiconductor quantum dots due to their size, tunable fluorescence, high quantum yield and wide excitation wavelength range have generated increasing interest among researchers in the past ten years. In 1994, Bawendi et al [21] reported the use of CdSe/TOPO nanocrystals in a thin film device.

1.1.2.1 Optoelectronic Applications

The surface area of a nanocrystal and the surrounding medium such the capping reagent can have a profound effect on the properties of the particle [17]. Defects within the particle act as electron/hole traps which can lead to nonlinear optic effects [22]. New nonlinear composite materials can be prepared by doping either polymers or glasses with semiconductor nanocrystallites [23].

1.1.2.2 Catalysis

The large surface area-to-volume ratio, along with the ability to tune the band gap by changing particle size, means that monodispersed semiconductors can be used as catalysts in photochemical reactions. The redox levels of the conduction and valence bands are especially sensitive to size quantization effects; with charge carriers formed after light absorption migrating to the surface of the particles where they can reduce or oxidize surface-bound chemical species [24]. For example, Henglein et al. reported the use of ZnS nanoparticles for oxidation of alcohols and the reduction of CO_2 to formic acid [25].

1.1.2.3 Sensing/Labelling

There has been great interest in this area including biological and chemical sensing [26]. For example, Kumar and Sberveglieri reported that TiO_2 nanoparticles can be used as sensors for the detection of O_2, NO_2 and organic molecules [27-28]. The selectivity of the sensor depends on the method used to produce the TiO_2 nanoparticles, with the efficiency of the chemical sensors increasing with decreasing particles size decreases. Nazzal et al. [26] found the photoluminescence of polymer thin films incorporated with high-quality CdSe nanocrystals respond rapidly to amine gases under photoirradiation.

Another active area is biological sensing. Chan et al [29] used CdSe/ZnS QDs modified with a protein transferrin to label HeLa cells through receptor-mediated endocytosis. They demonstrated that the attached transferring molecules were still active and recognized by the receptors on the cell surface. Their report also showed that when QDs labeled with IgG incubated with bovine serum albumin (BSA) and a specific polyclonal antibody, the polyclonal antibody recognized the Fab fragments of the IgG and induced an extensive aggregation of CdSe/ZnS QDs. In another report, Jaiswal et al. [30] demonstrated that QDs could be used for multiple-color imaging of live cells (Figure 3).

The labeling did not affect the normal growth and development of live cells, and have no obvious effect on cellular functions. Luminescent quantum dots also can be applied in quantitative bioanalysis. In protein and DNA chips, organic dyes have been widely used for drug screening and disease diagnostics. However, poor photostability and overlaps between emission peaks have been a problem. To overcome this problem, quantum dots have been explored as alternative of organic fluorophores in immunoassays and DNA analysis. Goldman et al. [31] prepared QDs-antibody conjugates and used them in fluoroimmunoassays for the detection of protein toxin and TNT with detection limits of 10 ng/ml for the toxin and 2 ng/ml for TNT.

Han et al. [32] encapsulated CdSe/ZnS QDs into 1.2 μm porous polystyrene microbeads with different ratios of quantum dots of different emission colors and formed barcodes for DNA hybridization assays. They prepared quantum dots of six different emission colors and doped them into polymer beads with 10 different ratios of emission intensity. The QDs doped polymer beads could be used to analyze one million DNA samples in a single detection assay.

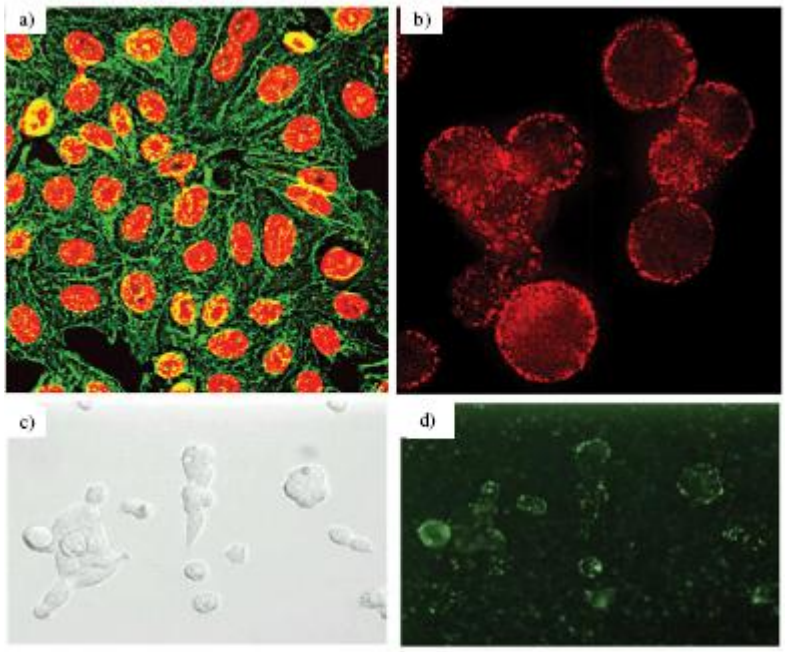

Figure 3. Labelling of fixed cells with bioconjugated quantum dots [33]

1.2 Magnetic Nanoparticles

1.2.1 Superparamagnetism

Superparamagnetism is the phenomenon, where magnetic materials exhibit paramagnetic behavior below a certain temperature, called Curie temperature. Above Curie temperature, the spins of the atoms in the lattice are out of alignment, due to high energy expressed in the form of vibrations. This misalignment results in paramagnetism. In this state, each individual atom retains its net magnetic dipole moment, but the combined effect does not result in a distinct average moment per molecule. However, when an external magnetic field is applied, atom spins align

accordingly and the combined effect results in a net magnetic moment for the molecule.

A distinct feature of paramagnetism, in contrast to ferromagnetism, is disappearance of the alignment and the associated magnetic effect with the removal of the magnetic field. In superparamagnetism, the material is confined in small space about 1-10 nm, and has no individual magnetic domain. Therefore, even small amounts of thermal energy observed below Curie temperature can disrupt alignment of spins and produce a zero net magnetism. Furthermore, the reaction to an applied magnetic field is stronger compared to paramagnetic materials.

This size dependent property has been observed for ferromagnetic materials like Fe_3O_4 and γ-Fe_2O_3 at dimensions below 15 nm. The derivative of iron with cobalt, chromium, nickel, copper and zinc are also hot investigation topic in this field [34].

1.2.2 Superparamagnetic Iron Oxides Nanoparticles (MNPs)

The general structure of an MNP consists of a core, surrounded by a shell. In this arrangement, the magnetic iron oxide core provides the magnetic properties, while the shell provides stability to the structure and determines the behavior in carrier liquid. Different applications may require different carrier liquids, and the shell structure should be adjusted accordingly. This is crucial, as application requirements show a wide variety. With the advancement in the technology, it has become feasible to design and manufacture nanoparticles specifically designed for biomedical applications [35-37].

With proper surface coating, these magnetic nanoparticles can be dispersed into suitable solvents, forming homogeneous suspensions, called ferrofluids [38]. Such a suspension can interact with an external magnetic field and be positioned to a specific area, facilitating magnetic resonance imaging for medical diagnosis and AC magnetic field-assisted cancer therapy [39]. Furthermore, it is possible to employ them in more direct interactions, such as hyperthermia, magnetofection and tissue repair [40-41].

Stable dispersion of magnetic nanoparticles in a solvent is crucial for many applications. At the nanoscale, this is hard to achieve, as nanoparticles are characterized by large surface/volume ratios, and consequently tend to aggregate in order to reduce the surface energy. The agglomeration is increased by the additional magnetic dipole-dipole attractive forces between nanoparticles [42]. Therefore, coating the magnetic crystal is very crucial. To begin with, coating determines the surface properties and affects the stability of their colloidal dispersions. Stability can be achieved by electrostatic and/or steric stabilization through the careful selection of coating molecules, such as organic surfactants and polymers. Functionalized water soluble block copolymers, combining water solubility, provided by hydrophilic block segment, with ability to bind to magnetic nanoparticles, provided by functionalized segment, offer an effective solution [43, 44]. Exactly this issue has been the triggering element of the grown interest in the development of new inorganic/organic hybrid structures. Thanks to the living/controlled polymerization methods, hybrid nanoparticles with tailored functionalities could be synthesized leading to the advanced materials. Among many approaches for coating the surface of nanoparticles with a shell of organic polymers using different living/controlled polymerization techniques, the surface initiated atom transfer radical polymerization (ATRP) has become a method of choice recently.

1.3 Atom Transfer Radical Polymerization (ATRP)

The name of atom transfer radical polymerization (ATRP) comes from the atom transfer step, which is the key elementary reaction responsible for the uniform growth of the polymeric chains. ATRP is one of the most widely used controlled/living free radical polymerization techniques and seems to be the most versatile one. This technique can successfully be applied to the living radical polymerization of methacrylates, acrylates and styrene monomers with well-controlled molecular weights and well-defined structures [45, 48].

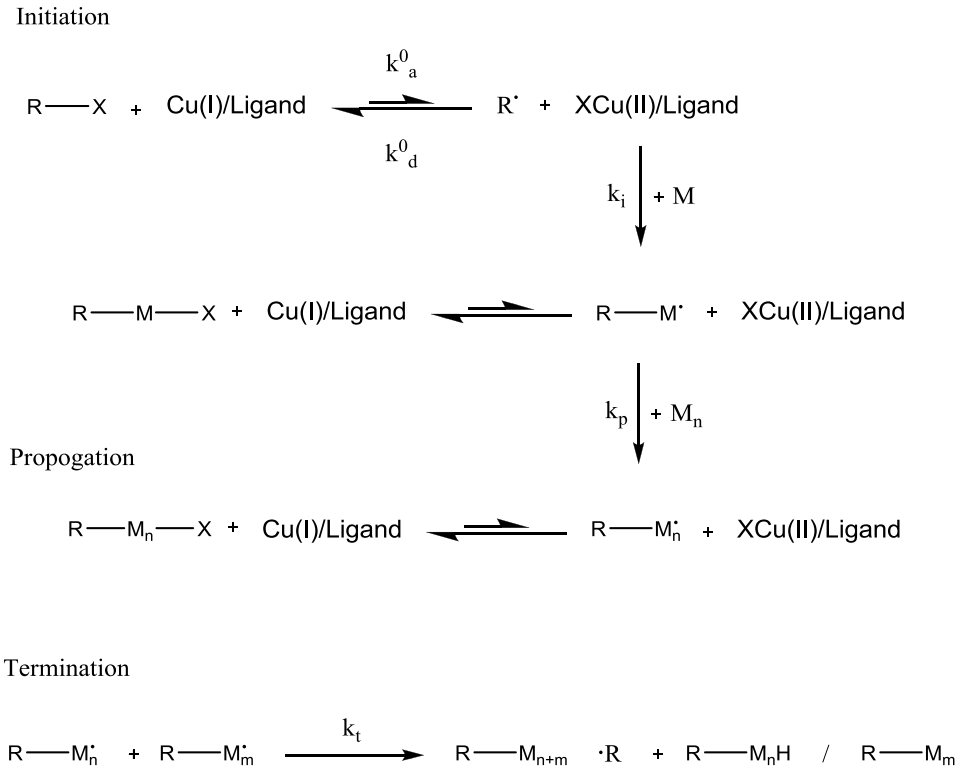

Figure 4. Flow of ATRP reaction [49]

As a multicomponent system, ATRP includes the monomer, an initiator with a transferable halogen, and a catalyst (composed of a transition metal species with any suitable ligand). Both activating and deactivating components of the catalytic system must be simultaneously present. Sometimes an additive, such as a Lewis Acid is used. For a successful ATRP, other factors, such as solvent, temperature, concentrations and solubility of all components, and sometimes the order of their addition must be also taken into consideration.

1.3.1 Kinetics of ATRP

The "living" character denotes the ability of further addition of monomer after consumption of initial batch and means that polymer chains do not undergo irreversible chain breaking reactions such as chain transfer or termination. Control aspect in the polymerization via ATRP method comes from the fact that the rate of chain initiation is fast compared with the rate of chain propagation, so that the number of kinetic chain carriers is essentially constant during the polymerization

leading to narrow molecular weight distribution, then synthesis of polymers with predetermined molecular weights and narrow molecular weight distribution becomes possible.

A sign of control in the polymerization via ATRP is that the polymerization rate (R_p) with respect to the log of the monomer concentration ([M]) is a linear function of time (Equation 5) [49]. This is due to the negligible contribution of non-reversible termination, so that the concentration of the active propagating species ([P*]) is constant. The rate of polymerization is first order with respect to monomer, alkyl halide (initiator), and transition metal complexed by a ligand (Equation 6) [49]. The reaction is usually negative first order with respect to the deactivator (CuX_2/Ligand).

$$R_p = \frac{-d[M]}{dt} = k_p[P^*][M] \tag{5}$$

$$R_p = k_{app}[M] = k_p[P^{\cdot}][M] = k_p K_{aq}[I]_0 \frac{[Cu(I)]}{[Cu(II)X]}[M] \tag{6}$$

Results from kinetic studies of ATRP for styrene, methyl acrylate (MA), and methyl methacrylate (MMA) under homogeneous conditions indicate that the rate of polymerization is first order with respect to monomer, initiator, and Cu(I) complex concentrations [49].

If the deactivation does not occur or if it is too slow ($k_p >> k_d$), there will be no difference between ATRP and the classical redox reactions and the termination and transfer reactions may be observed. To gain better control over the polymerization, addition of one or a few monomers to the growing chain in each activation step is desirable. The polymer chain-length distribution defined as molecular weight distribution or polydispersity (M_w/M_n) is an indicator of the control over the polymerization.

$$\frac{M_w}{M_n} = 1 + \left(\frac{k_p[RX]_0}{k_d[XCu(II)]}\right)\left(\frac{2}{p} - 1\right) \quad (7)$$

p = polymerization yield
$[RX]_0$ = concentration of the functional polymer chain
[XCu(II)] = concentration of the deactivators
k_d = rate of deactivation

Equation 7 illustrates how the polydispersity index in ATRP relates to the concentrations of initiator (RX) and deactivator (XCu(II)), the rate constants of propagation (k_p) and deactivation (k_d), and the monomer conversion (p) [49]. This equation holds for conditions when initiator is completely consumed and degrees of polymerization are sufficiently high; otherwise the Poisson term should be added (1/DP*n*). Thus, for the same monomer, a catalyst that deactivates the growing chains faster will result in polymers with lower polydispersities (smaller k_p/k_d). For example, the addition of a small amount of Cu(II) halides in the copper-based ATRP leads to better controlled polymerizations with decreased polymerization rates. Another implication of Equation 3 include higher polydispersities for shorter chains (higher $[RX]_0$) and a decrease of the polydispersity with increasing monomer conversion.

1.3.2 Monomers

A variety of monomers have been successfully polymerized using ATRP; styrenes, (meth)acrylates, (meth)acrylamides, acrylonitrile, N-vinylpyridine, and diens, which contain substituents that can stabilize the propagating radical. The polydispersity of the polymers obtained via ATRP technique is usually between 1.05 and 1.5.

1.3.3 Initiators

The main role of the initiator is to determine the number of growing polymer chains. In ATRP, alkyl halides (RX) are typically used as initiators. To obtain well-defined polymers with narrow molecular weight distributions, the halide group, X, should rapidly and selectively migrate between the growing chain and the transition metal complex. When X is either bromine or chlorine, the molecular weight control is the

best. The initiator usually, but not always, should have a structure homologous to the corresponding polymer end group.

1.3.4 Ligands

Main role of the ligand in ATRP is to solubilize the transition metal salt in the organic media and to adjust the redox potential and halogenophilicity of the metal center forming a complex with an appropriate reactivity and dynamics for the atom transfer. The ligand should complex strongly with the transition metal. The most widely used ligands for ATRP systems are the derivatives of 2,2-bipyridine and nitrogen based ligands such as N,N,N',N'',N'' pentamethyldiethylenetriamine (PMDETA), Tetramethylethylenediamine (TMEDA), 1,14,7,10,10 hexamethyltriethylenetetraamine (HMTETA), tris [2-(dimetylamino) ethyl]amine (Me-TREN) and alkylpyrdylmethanimines are also used (Figures 5 and 6).

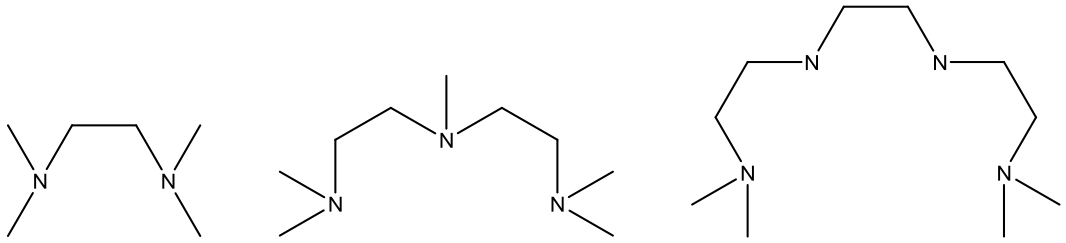

TMEDA PMDETA HMTETA

Figure 5. Nitrogen based ligands

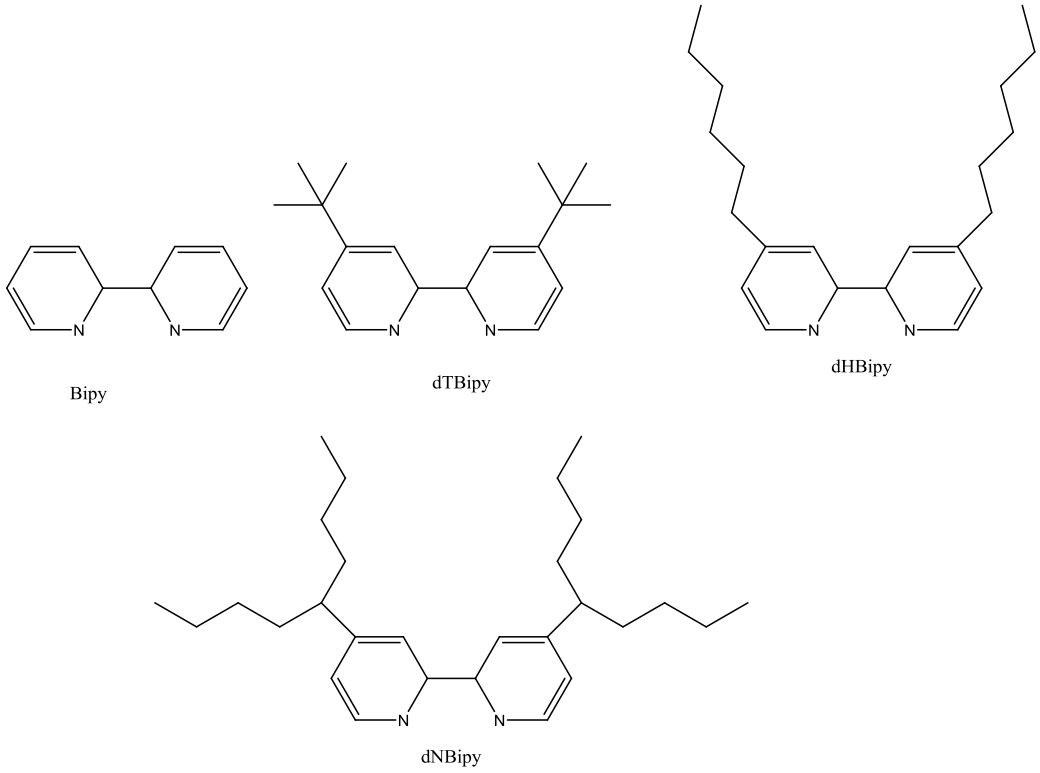

Figure 6. Derivatives of 2,2-bipyridine

1.3.5 Transition Metal Complexes

The most important component of ATRP is the catalyst. There are several prerequisites for an efficient transition metal catalyst. First, the metal center must have at least two readily accessible oxidation states separated by one electron. Second, the metal center should have a reasonable affinity towards a halogen. Third, the coordination sphere around the metal should accommodate a halogen upon oxidation. Fourth, the ligand should complex the metal relatively strongly. The most important catalysts used in ATRP are Cu(I)Cl, Cu(I)Br, $NiBr_2$ $(PPh_3)_2$, $FeCl_2$ $(PPh_3)_2$, $RuCl_2$,$(PPh_3)_3$ / $Al(OiPr)_3$.

1.3.6 Solvents

ATRP can be carried out either in bulk, in solution, or in a heterogeneous system (e.g., emulsion, suspension). Various solvents, such as benzene, toluene, anisole, diphenyl ether, ethyl acetate, acetone, dimethylformamide (DMF), ethylene

carbonate, alcohol, water, carbon dioxide, and many others, have been used in the polymerization of different monomers.

1.4 Purpose of the Research and Objectives

The aim of this study is the synthesis of hybrid nanoparticles, composed from two different nanoparticles with distinct properties, in a layered structure where the distance between them can be controlled. Specifically, the combination of superparamagnetic and luminescent quantum dots is targeted.

The block copolymerization via ATRP is selected as the method of synthesis. The polymers start growth from the surface of a nanoparticle(MNP), where first block determines the distance between two particles and the second block provides stability and coating to the second nanoparticle (QD). The final product has the ability to react to both magnetic fields and UV stimulation. Such a structure can be used in medicine (both diagnosis and therapy), multifunctional sensors, magnetic separation, magnetic/optic imaging and optic labeling.

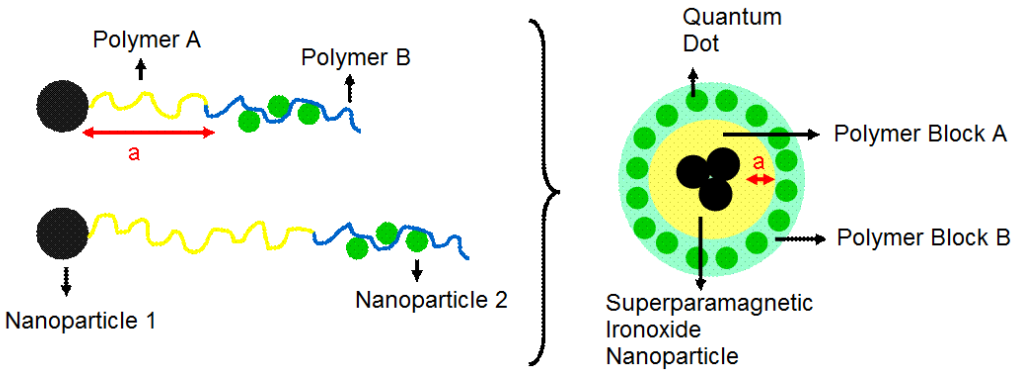

Figure 7. The schematic representation of hybrid structures

The novel contribution of this study is the control over distance between two types of nanoparticles in hybrid structures. This ability allows, for the first time, the examination of the relation between particle distance and light emission, revealing the distance for optimum luminescence. After the determination of the underlying mechanism, the effects of distance on emission quality can also be used as a sensory mechanism. Therefore, this study also aims to design hybrid nanoparticles joined by

pH or temperature sensitive polymer blocks, able to reflect state of the environment in their emission quality, acting as a sensor.

Unfortunately, iron oxides absorb light at the wavelength range where quantum dots emit. Therefore, the light emission from hybrid structures combining these nanoparticles has poor quality. Until now, this drawback is largely disregarded. However, based on the strategy provided in this work, it is possible finely tune emission properties. As a result, the work presents a method to overcome this deficiency. Consequently, this study establishes a valuable methodology for the strictly controlled integration of different nanoparticles.

In conclusion, the aim of this study consists of several objectives, namely, synthesis of nanoparticles with poylmer initiators on their surface, controlled block copolymerization from nanoparticle surface via ATRP, detailed study of polymerization character.

Chapter 2 SYNTHESIS OF SURFACE MODIFIED MAGNETIC NANOPARTICLES (MNPs)

2.1 Introduction

Superparamagnetic iron oxide (SPIO) nanoparticles have a wide range of applications, including but not limited to ferrofluids, contrast enhancement in magnetic resonance imaging, and magnetic separation of biological and mineral entities. In recent years, coating MNP surface with polymeric materials became one of the most popular methods to alter the surface chemistry and function of the nanoparticles. Some of the most exploited functions of MNPs include sensing, detecting, labeling and dragging as a response to the external magnetic field [50-54]. Chemical nature of the polymer can influence these functions. For practical purposes, however, the polymer shell is required to have a good stability and high concentration of functional groups. For biological/medical purposes it has to be non-toxic as well. For much better control of particle properties, such as shell thickness, a precise control of the polymer properties can be desired such as uniform chain-length distribution and controlled molecular weight.

There are several methods developed for the coating of nanoparticles with polymers such as physical adsorption of polymers on nanoparticles, emulsion polymerization in the presence of nanoparticles, and the so-called '*grafting-to*' and '*grafting-from*' methods [55-58]. The '*grafting-from*' approach is a promising candidate to achieve a tightly bound stable polymer layer on the nanoparticle surface and a high graft density.

A recent success in this field is the application of living polymerization techniques to surface-initiated graft polymerization for the preparation of a dense polymer layer with controlled structures [56-63]. Among many approaches for coating the surface of nanoparticles with a shell of organic polymers, the surface initiated atom transfer radical polymerization (ATRP) has become a method of choice due to its applicability to a large variety of monomers and relatively simpler procedure.

Furthermore, it is one of the most straightforward ways to synthesize block copolymers, paving the way for a universal method for the synthesis of hybrid nanostructures.

A crucial step to achieve ATRP from MNP surface using *grafting-from* strategy is the synthesis of functionalized initiators. In ATRP, alkyl halides (RX) are typically used as the initiator and the rate of the polymerization is first order with respect to the concentration of RX. To obtain well-defined polymers with narrow molecular weight distributions, the halide group, X, must rapidly and selectively migrate between the growing chain and the transition-metal complex. In general, any alkyl halide with an activating substituent on the R-carbon, such as aryl, carbonyl, or allyl groups, can potentially be used as ATRP initiators. The initiating moiety could be attached to flat surfaces, nanoparticles or macromolecules [64].

This step is crucial, since unsuccessful immobilization of initiator on the surface may result in the low concentration of initiator in the system which may in turn lead to problems such as rapid increase in molecular weight or high polydispersity during polymerization step or instability/insolubility of nanoparticles.

Recently, several groups have reported different approaches for the immobilization of ATRP initiators on the surface of nanoparticles. Successful polymerizations from nanoparticles typically require the covalent attachment of initiators, which form monolayers that accelerate particle dispersion and mitigate polymer bridging. Recently, some groups have reported the trialkyloxysilane or trichlorosilane based initiators to be covalently bonded on the surface of MNPs through sol–gel method [65]. A common drawback of this method is the high trend to selfcondensation of the trialkoxysilane or trichlorosilane.

In this study, the surfaces of MNPs are functionalized by two different approaches, namely Ligand Exchange and one pot synthesis in DMF. The ligand Exchange is a well-known and efficient method in the nanoparticle solubilization and functionalization. In this method, fatty acid coating of nanoparticles are exchanged by the trialkoxysilane functionalized ATRP initiator. Recently Wang et al. [66] has utilized a solvent-free ATRP approach for the synthesis of the core/shell

nanoparticles, in which iron oxide cores became soluble in styrene after ligand exchange with 2-bromo-2-methylpropionic acid. Condensation of alkoxysilane groups with the surface Fe-OH groups forms a covalent bond between the initiator and the MNP rendering nanoparticle stable. These covalently attached initiators offer a great advantage over physically or chemically adsorbed initiators in terms of stability.

On the other hand, one pot synthesis in DMF is a novel, promising and straightforward method for the immobilization of initiator molecules to the NP surface. This involves synthesis of iron oxide nanoparticles in DMF from the iron salts in the presence of the ligand which in this case has an ATRP initiator moiety. The major advantage of this approach is that it is a single step approach to produce initiator coated MNPs which saves time, money, energy. Besides and may be more importantly, since several precipitation or ligand exchange steps will be excluded, aggregation events due to processing will be eliminated and whatever is attached on the particle surface will be an initiating moiety. Moreover, relying on our experience on the subject, we know that after ligand exchange the MNPs acquire a much more hydrophobic character, but the halogen tail of the initiator still causes the particles to be relatively polar; so, as a highly hydrophilic organic solvent, DMF becomes a perfect candidate for the direct synthesis of MNPs. For both approaches, we used two different alkoxysilane initiators as shown in Figure 8 and Figure 9.

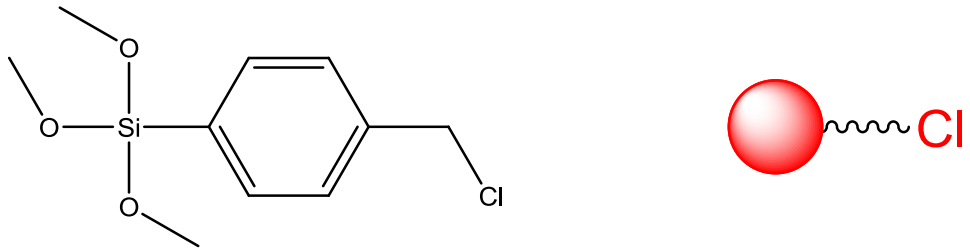

Figure 8. p-chloro methyl phenyl trimethoxysilane

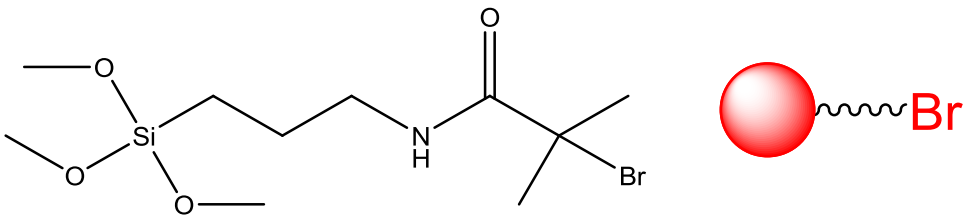

Figure 9. 2-bromo propionamide propyltrimethoxysilane

These initiators consist of an alkoxysilane anchoring group, an aliphatic spacer, and an ATRP initiator group (halogen).

CPTMS, which is a primary chloride initiator, has a dramatically lower activation rate than BPTMS, which is a tertiary bromide initiator [64]. The use of MNPs functionalized with different initiator groups alters the kinetics of polymerization.

2.2 Experimental Section

2.2.1 Materials

All reagents were used as received unless indicated otherwise. $FeCl_3.6H_2O$, $FeCl_2.4H_2O$ and lauric acid (LA) were purchased from Fluka. Ammonium hydroxide (26% NH_3 in water, w/w) was purchased from Riedel-de Haen, p-chloromethylphenyl trimethoxysilane (CMPTS), 3-Aminopropyltriethoxysilane (APTMS) were purchased from Gelest. Toluene and dimethylformamide (DMF) were purchased from Merck. 2-bromoisobutyryl bromide and triethylamine (TEA) were purchased from Aldrich Chemical. Dialysis bag with MWCO 3500 was purchased from CelluSep.

2.2.2 Synthesis of the 2-bromo Propionamide Propyltrimethoxysilane (BPTMS)

Toluene (10 mL) with 2-bromoisobutyryl bromide (0.1 mL, 0.8 mmol) was added dropwise to a cold solution of APTMS (0.18 mL, 0.8 mmol) in dry toluene (10 mL) with TEA (0.12 mL, 0.8 mmol) at 0°C. The mixture was magnetically stirred for 3 h at 0°C and then for another 10 h at room temperature. The mixture was passed through a filter paper to remove the salts and the filtrate was evaporated to remove

the unreacted TEA under reduced pressure. BPTMS was obtained as a colorless viscous liquid in 80% yield.

2.2.3 Synthesis of Initiator Coated MNPS by the Ligand Exchange

2.2.3.1 Preparation of LA Bilayer Coated MNPs

45 mL of distilled water was put into a 100 mL three-necked round bottom flask fitted with a mechanical stirrer and a condenser and deoxygenated for 30 minutes. Iron salts ($Fe3^{+}$ / Fe^{2+} mole ratio of 2), lauric acid were added to the flask and stirred at 400 rpm under nitrogen for about 15 minutes.

Then, reaction flask was placed into an oil bath at 85°C. After 10 minutes of mixing, ammonium hydroxide was injected to the flask with vigorous stirring at 600 rpm. Reaction was allowed to continue for 30 minutes to produce a stable colloidal solution, then cooled to room temperature and placed atop a magnet (0.3 Tesla) for few hours. Any precipitate was removed with magnetic decantation.

2.2.3.2 Preparation of LA Monolayer Coated MNPs by Extraction Method

10 ml of dark brown colloidal suspension (LA bilayer coated iron oxide) was mixed with 20 ml of toluene and shaken well. After the equilibrium was reached, the dark brown chloroform layer with the monolayer coated particles was separated. In order to speed up the extraction, a small amount of isopropanol was be added into the solution. The toluene layer was dried with molecular sieves.

2.2.3.3 Ligand Exchange

The following procedure was performed for both functional ligands, CMPTS and BPTMS. LA monolayer coated nanoparticles were stirred vigorously with excessive amount of functional ligand in 40 ml toluene mechanically under nitrogen at room temperature. After 1 hour stirring, NH4OH was injected. Reaction was allowed to continue for 30 minutes to produce a stable colloidal solution, and then placed atop a magnet (0.3 Tesla) for few hours.

Any precipitate was removed with magnetic decantation. Then, the particles were precipitated into hexane and washed with toluene twice. Particles were removed from the toluene by centrifugation (1h) at 50,000 rpm at room temperature. Cleaned particles were resuspended in DMF by sonication.

2.2.4 One Pot Synthesis in DMF

2.2.4.1 Experimental Procedure

29 mL of distilled DMF was put into a 100 mL three-necked round bottom flask fitted with a mechanical stirrer and a condenser and deoxygenated for 30 minutes. Iron salts (Fe^{3+} / Fe^{2+} mole ratio of 2) were added to the flask and stirred at 400 rpm under nitrogen for about 15 min.

Reaction flask was placed into an oil bath at 85°C. After 10 min of mixing, desired functional ligand was added to the flask. Afterwards, ammonium hydroxide was injected to the flask with vigorous stirring at 600 rpm. Ratios of the reactants are given in Table 1. Reaction was allowed to continue for 30 minutes to produce a stable colloidal solution, then cooled to room temperature and placed atop a magnet (0.3 Tesla) for a few hours. Any precipitate was removed with magnetic decantation. Both dialysis and precipitation strategies are employed in order to get rid of the unreacted free initiator. In removal by dialysis method, nearly 30 ml of MNP solution was transferred to a dialysis bag submerged in 300 ml of DMF and vigorously stirred overnight. In removal by precipitation method, the particles were precipitated into hexane. Then, fresh toluene were added to the precipitated nanoparticles, sonicated briefly and precipitated by 1h centrifugation at 50,000 rpm at room temperature.

Table 1. Reaction Conditions of MNP Synthesis

Total Fe (mol)	Fe^{3+} /Fe^{2+} (mol ratio)	Total Iron conc. (M)	Si/Fe (mol ratio)	Base ratio
0.009	**2**	**0.25**	**0.5**	**2**

2.2.5 Instrumentation

FTIR spectra were recorded on Jasco FT-IR-600 spectrometer. Hydrodynamic sizes of the nanoparticles were measured as intensity, number and volume average on a Malvern Zetasizer Dynamic Light Scattering Unit. Thermal gravimetric analysis (TGA) was performed on a Seiko SSC 5200 TG/DTA at a scan rate of 10°C min^{-1} up to 600°C under nitrogen atmosphere.

2.3 Results and Discussion

2.3.1 Functional Ligand Synthesis

It is well established that trialkoxysilane molecules hydrolyze, oligomerize, and finally condense with hydroxyl groups present at the surface of oxide particles [67]. For the immobilization of a tertiary bromide containing ATRP initiator on the MNP surface, BPTMS was synthesized in a simple amidation reaction from aminopropyl trimethoxysilane and 2-bromoisobutyryl bromide (Figure 10). The structure of BPTMS was confirmed by IR and 1H-NMR measurements (Figures 11 and 12).

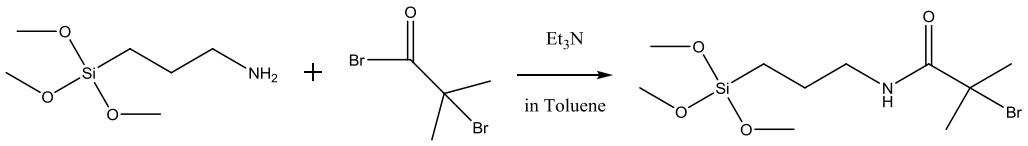

Figure 10. BPTMS synthesis pathway

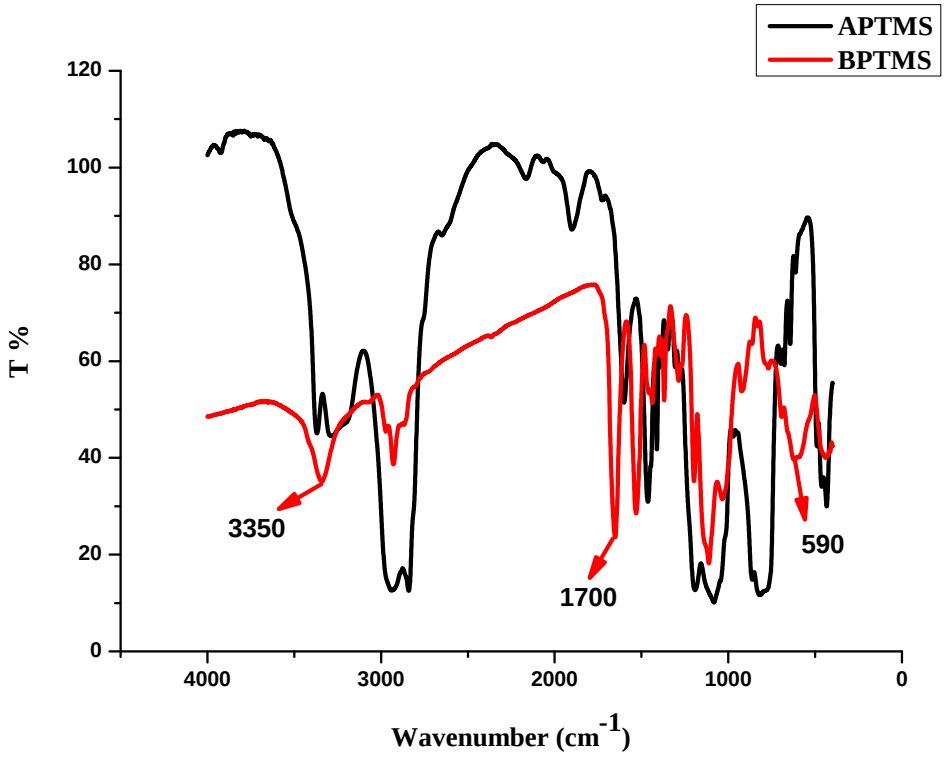

Figure 11. FT-IR spectrum of APTMS (black) and BPTMS (red)

As shown in Figure 11, characteristic primary amine stretching which usually shows two N-H peaks at around 3350 cm, turns into a single secondary amine peak after the condensation reaction. This in addition to the appearance of a carbonyl peak at 1700 cm^{-1} confirms amidation. The band around 590 cm^{-1} corresponds to C-Br vibrations of the initiator.

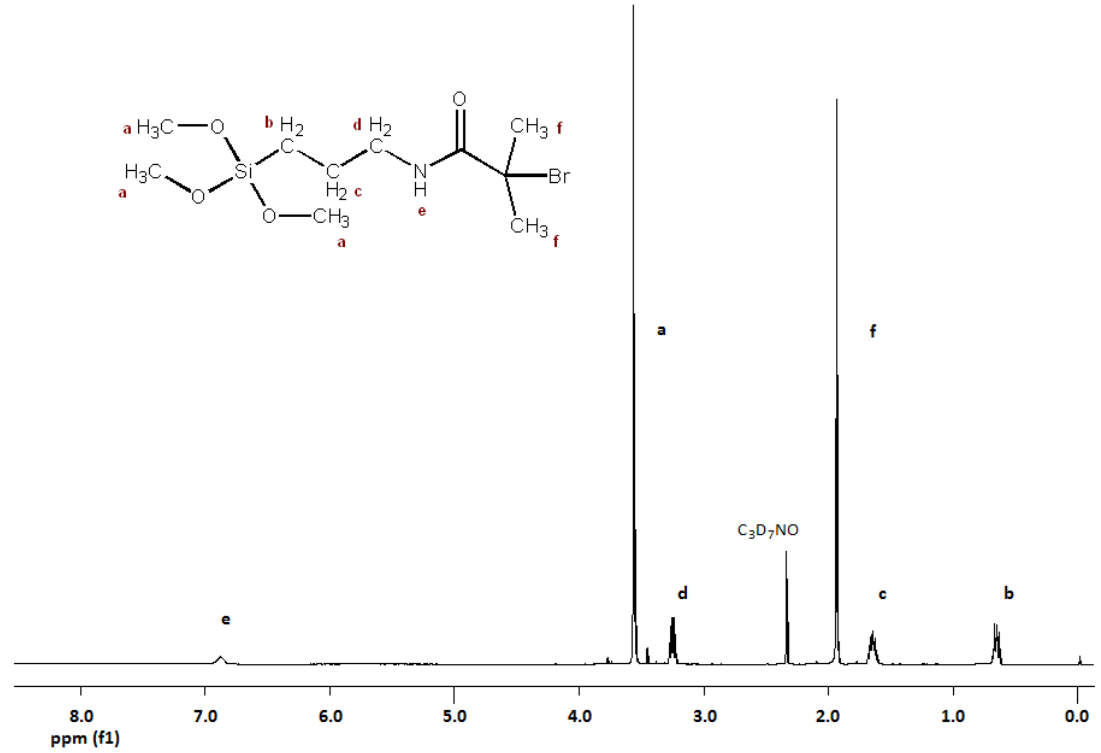

Figure 12. H-NMR spectrum of BPTMS

2.3.2 LA Coated MNPs

Lauric acid (LA) stabilized iron oxide nanoparticles were synthesized from aqueous solution of iron salts with NH_4OH in the presence of excess amount of LA. Aqueous suspension of nanoparticles is formed as the lauric acid organizes in an interdigitated bilayer around the nanocrystal surface [68, 69]. Removal of the second surfactant layer by alcohols provide LA monolayer coated hydrophobic nanoparticles that can be dispersed in toluene and chloroform as reported by Yagci et al [69].

Based on the previous studies of our group, we already know that LA monolayer coated MNPs can be obtained either by precipitation or extraction method, on the other hand extraction method is a better choice in order to obtain smaller particles [70]. LA monolayer coated particles were extracted from the initial aqueous suspension of the bilayer-coated particles with toluene (Figure 13). In the extraction process, phase separation was quite slow. In order to decrease the equilibrium time of

the extraction, we have added a small amount of isopropanol (IPA). The suspension in toluene of LA coated MNPs made further steps easier.

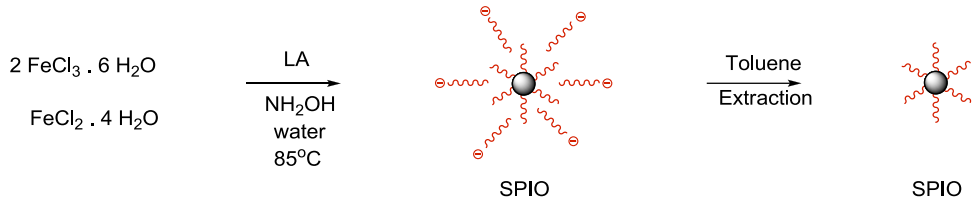

Figure 13. Schematic for preparation of LA coated MNPs

2.3.3 Ligand Exchange

One of the most efficient and widely studied ways to obtain halogen ended MNPs is Ligand Exchange, namely exchanging the original ligand adsorbed on the NP surface with a new ligand which carries the halogen functionality. Both CMPTS (p-chloro methylphenyl trimethoxysilane) and BPTMS (bromo propyl trimethoxysilane) ligands were used to exchange LA from the MNP surface to create an initiator coated MNP for surface initiated ATRP polymerization of various monomers from the MNP surface. Base catalyzed hydrolysis of alkoxysilane units at room temperature in toluene created Fe-O-Si bonds that anchors the initiator to the surface of the iron oxide and intermolecular condensation creates a thin Si-O-Si skin, both of which enables a very stable coating around MNP. This is very important in order not to lose the initiating sites from the surface at the later stages.

Halogen ended MNPs were not very stable in toluene after ligand exchange, since Cl tail of the initiator causes the particles to be relatively polar. So MNPs were precipitated into hexane, washed and resuspended in DMF which provides a stable suspension.

Dynamic Light Scattering results show that the particle size is decreased after ligand exchange process for both functional ligands suggesting a breakdown of loose aggregates.

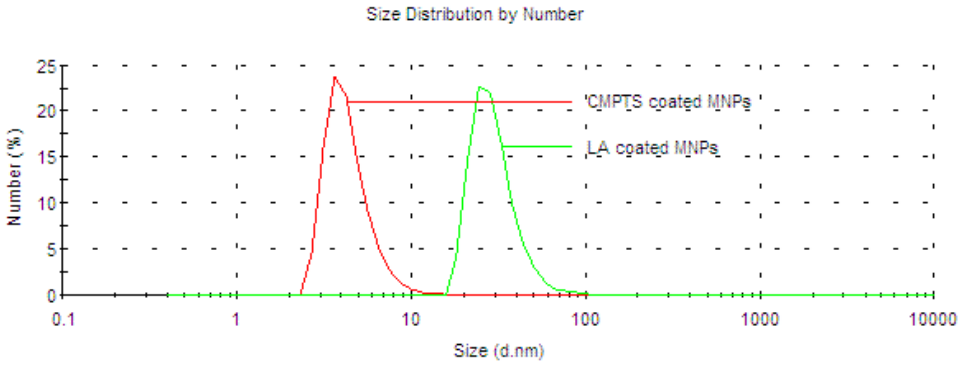

Figure 14. Size distribution of LA and CMPTS coated MNPs in DMF measured by DLS

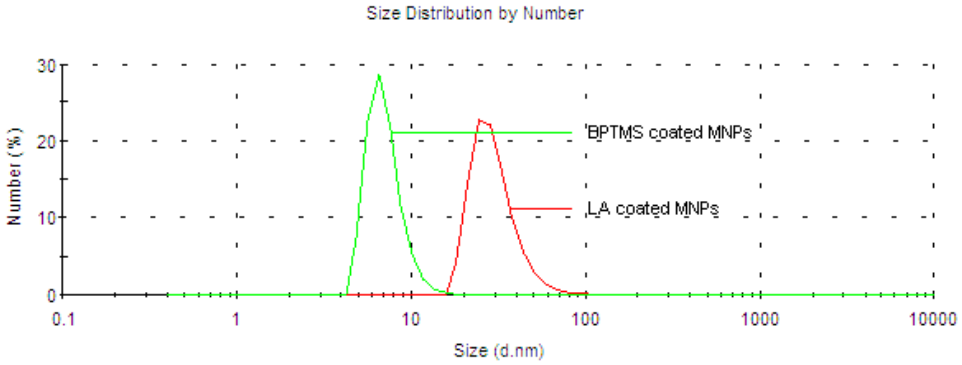

Figure 15. Size distribution of LA and BPTMS coated MNP in DMF measured by DLS

FT-IR analysis was performed to determine the surface composition of the resulting MNPs. The spectrum shows characteristic absorption bands of LA on the MNPs surface. The 1580 cm^{-1} and 1450 cm^{-1} bands belong to the presence of coordinated COO^- groups of LA with Fe_3O_4, which confirm the bonding of the LA ligand to the surface of MNPs through COO^- functionality.

Similar results of the COO^- group band were also observed for OA adsorbed on cobalt nanoparticles [66] and Fe_2O_3 nanoparticles [71].

As shown in Figure 16, after surface modification via ligand exchange, the typical alkyl stretching peak at 3000 cm^{-1} disappears significantly for both functional ligands.

In the case of BPTMS coated MNPs the N–C=O bond appears at 1643 cm^{-1} and 1544 cm^{-1}. The large band around 1000 cm^{-1} corresponds to Si–O–Si vibrations and attests to the formation of a silica layer. Moreover, the secondary amine peak, that appears around 3350 cm^{-1} after ligand exchange, shows the successful binding of BPTMS on MNPs.

The most important peak was at 700 cm^{-1} indicating the presence of C-Cl bond in CPTMS. The other peaks that show the adsorption of CMPTS onto the particle were at 815, 996, 1031 and 1130 cm^{-1}, corresponding to OH vibrations, Si-OH and Si-O-Si groups in the case of BPTMS.

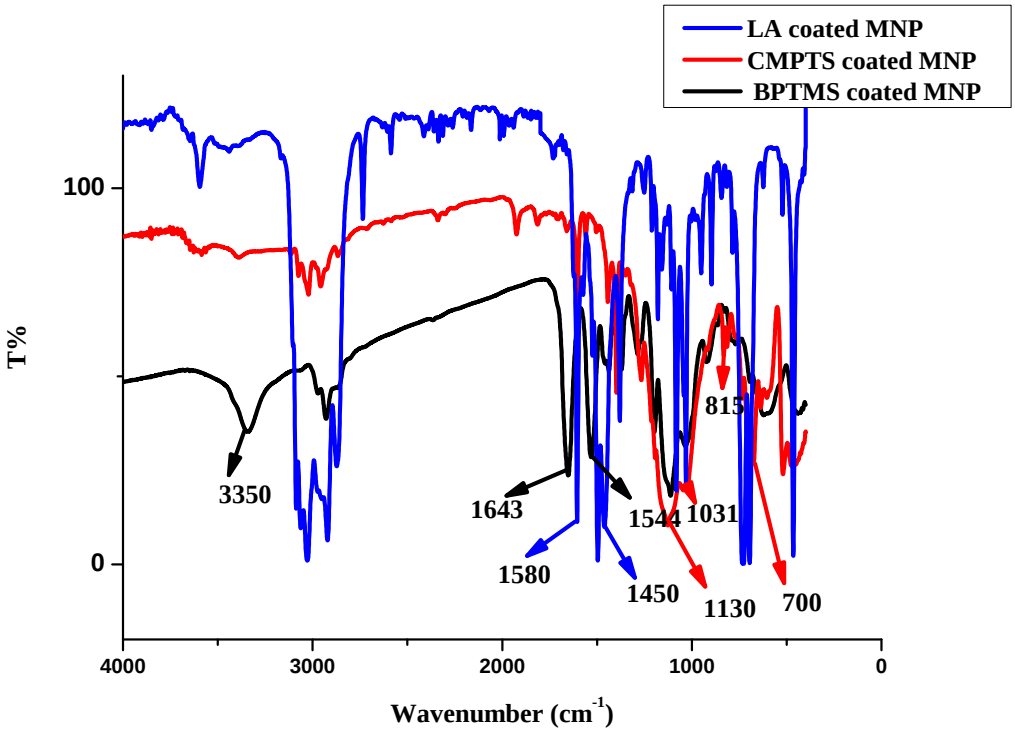

Figure 16. FT-IR spectrum of LA coated (a), BPTMS coated (b) and CPTMS coated (c) particles

Thermogravimetric analysis provides information about the coating as well (Figure 17). The bilayer coated particles showed two-step decomposition with 42% weight

loss at 180 °C and 14% at 280 °C. First decomposition step is due to the free LA and physically adsorbed outer layer and the second step at higher temperature is for the chemically and more strongly adsorbed inner layer. The monolayer coated particles had a 35% weight loss starting at about 180 °C which is plausible for the decomposition of the LA and a second 5% weight loss at 300 °C. BPTMS coated nanoparticles showed a 2% weight loss which is probably caused by solvent adsorbed on surface. Approximately 3% weight loss observed at 200 °C which may be attributed to the decomposition of LA that couldn't be completely removed in ligand exchange step. There is a 18% weight loss starting at about 360°C, which is believed to be due to the decomposition of the BPTMS. In addition, from the weight loss, the number of molecules per gr was calculated according to the following equation:

$$\#\ \text{of moles per gram} = \frac{\%\ \text{Organic Content}}{M_w^{\text{ligand}} \times 100} \tag{8}$$

The amount of anchored ligand on the MNP surface was calculated as $5{,}5.10^{-4}$ mol/gr according to the Equation 4.

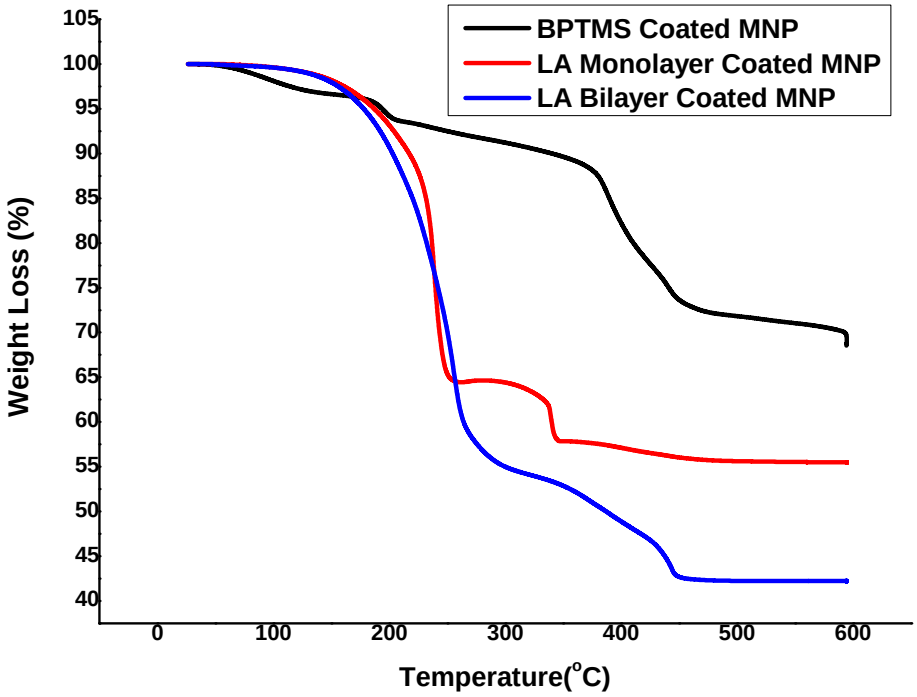

Figure 17. TGA data of BPTMS coated (a), LA monolayer coated (b) and bilayer coated (c) iron oxide nanoparticles

2.3.4 One Pot Synthesis in DMF

Direct synthesis of functionalized MNP in DMF is achieved with quite high organic content at around 44% (Figure 18). After the synthesis different strategies were undertaken to remove the unbound ligands which are actually the ATRP initiators: Dialysis and precipitation. DLS results showed a dramatic difference in hydrodynamic sizes of MNPs purified with dialysis and the ones subjected to precipitation and resuspension steps. Dialyzed particles were around 30 nm whereas the precipitated particles were around 100nm. This indicates that once precipitated aggregation is difficult to defeat which was observed in different studies as well. Magnetic interaction between the particles and the molecular interaction plays a role in this.

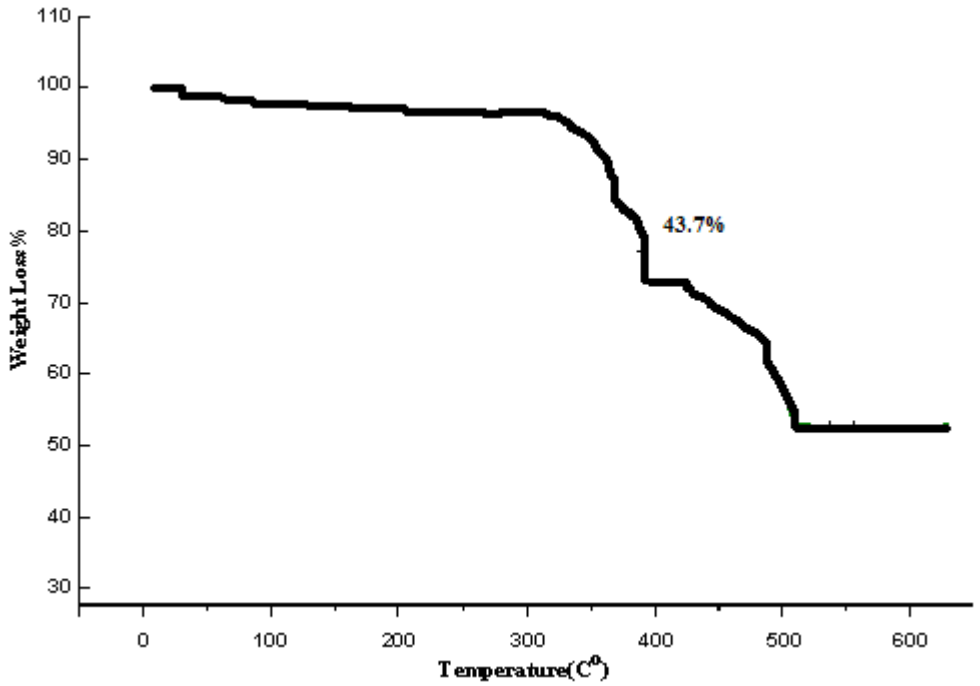

Figure 18. TGA data of CPTMS coated MNPs prepared by the one pot synthesis in DMF

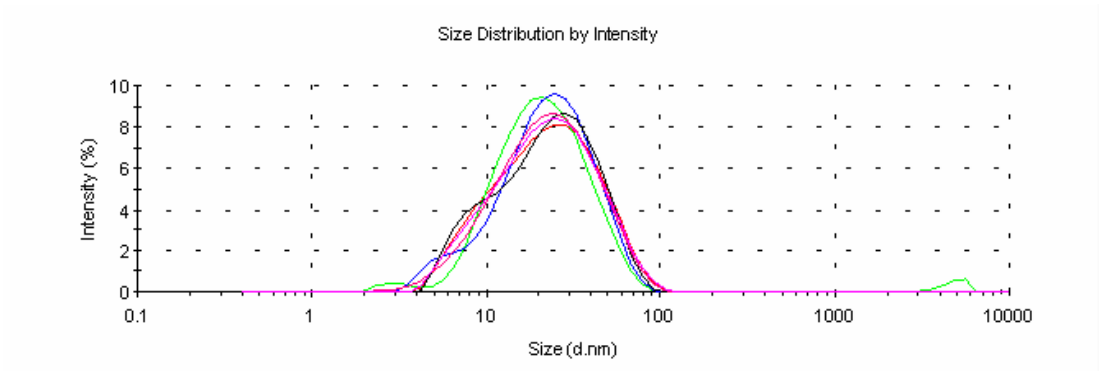

Figure 19. CMPTS coated MNPs after dialysis

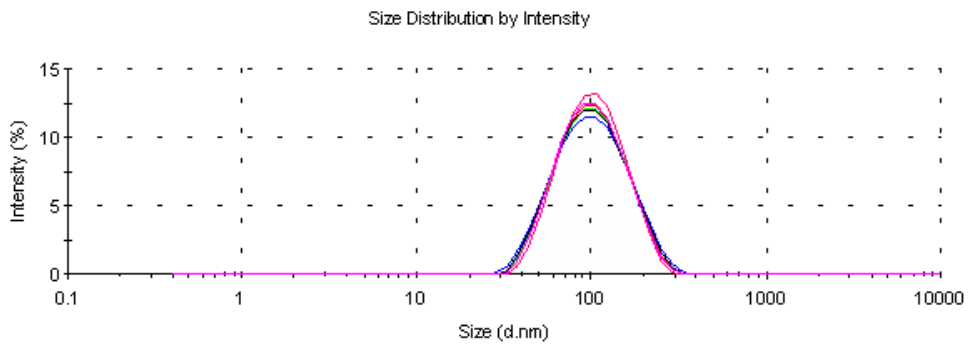

Figure 20. CMPTS coated MNPs after precipitation/resuspension

2.4 Conclusion

Surface functionalized MNPs with different initiator functionalities are synthesized via two different methods, namely ligand exchange and one pot synthesis in DMF. Ligands with a tertiary bromide and a primary chloride were chosen due to the availability of the later and higher activity of the former. Initiator moieties were anchored to the NMP surface through Si-O bonds. Structures were confirmed by FTIR. Hydrodynamic sizes of these particles are between 30-100 nm on average indicating small aggregates which are not unusual, yet size is influenced by the preparation method. Amount of initiator present on MNPs were calculated as $5{,}5.10^{-4}$ mol/g based on the TGA data. Overall, stable colloids of initiator functionalized MNPs in DMF was achieved for surface initiated ATRP polymerizations.

Chapter 3 APPLICATION OF SURFACE INITIATED ATRP TO MNP

3.1 Introduction

In the recent years, coating superparamagnetic iron oxide nanoparticles with organic polymers became quite popular, since polymers can be multifunctional and possess many different properties that will be suitable for various applications [72]. In addition to prevent the excessive aggregation of nanoparticles which have the tendency to form larger aggregates due to anisotropic dipolar attraction, this layer may also provide unique properties such as pH and temperature sensitiveness and biocompatibility. Among various techniques available for coating nanoparticle surfaces with a shell of organic polymers, the surface-initiated atom transfer radical polymerization (ATRP) stands out as the preferred method. Three major advantages of using the ATRP method are low polydispersity, control over molecular weight of polymers and active chain ends which allow block copolymer formation or end group functionalization. In principle, ATRP process involves a halogen transfer to a transition metal complex, resulting in the reversible redox activation of a dormant alkyl halogen terminated polymer chain end. The surface initiated ATRP ((SI)-ATRP) process is controlled by many parameters, such as type of the ligand, metal, solvent, initiator, as well as ligand to transition metal ratio or Cu(II) to Cu(I) ratio, and these parameters can be adjusted to tune polymer properties [72-76].

In literature, there are many studies about the synthesis of polymeric core/shell nanoparticles, such as SiO_2, Au, $MnFe_2O_4$ and Fe_2O_3, using ATRP [77-80]. However, the studies about surface initiated block polymerization are relatively rare. There are two approaches for surface initiated polymerization: *grafting-to* and *grafting-from*. As stated earlier in this study, *grafting-to* approach has several limitations, making synthesis of thick and very dense polymer brushes very difficult. In the *grafting-from* approach, however, the polymerization starts from the initiator-functionalized surfaces resulting in highly stabilized polymer layer and high graft density [81]. Controlled/living polymerization techniques, such as ATRP in our case,

are well suited to the synthesis of polymer brushes by *grafting-from* approach, because the process has finely tuned control over brush thickness, composition, and architecture [78].

Previous studies on the surface initiated ATRP showed that the addition of free initiator directly into the system increases the concentration of deactivating species and results in a better control in brush growth [82-84]. Furthermore these studies have shown that, the molecular weight of the polymer chains initiated by the free initiator in solution were approximately the same with the polymer chains grown from the surface [84]. Therefore, it is possible to use easily obtainable kinetic data from polymer grown in solution to estimate the molecular weight of the brush.

On the other hand, this approach, limits the maximum brush thickness, since some of the monomer will be used in the formation of polymer in solution. Furthermore, the free polymer must be removed from the brush once the polymerization is complete. A common solution to this problem is extracting the brush in a good solvent [84]. Precipitation of the nanoparticles is an alternative method that may be useful.

An alternative approach is also developed in order to obtain controlled brushes grown from the surface of nanoparticles. Instead of adding excess initiator, most of which will be consumed by growth in solution, deactivating Cu(II) can be added at the beginning of the polymerization [85-86]. As a result, the need for tedious methods to remove unbound polymers is eliminated. Using this principle by adding deactivating $CuBr_2$ directly to an aqueous HEMA polymerization, Huang et al. accomplished synthesis of 700 nm thick poly(2-hydroxyethyl methacrylate) (PHEMA) films [85], which is an extraordinary thickness for this product. Another related study by Matyjasewski et al. has confirmed the method by the synthesis of polystyrene (PS) brushes from bromoisobutyrate-functionalized silicon wafers [86].

Another strategy to increase the control over the reaction is halogen exchange method. Matyjaszewski concluded that the control can be increased by using mixed halide systems, as higher free energy of dissociation of the C-Cl compared to C-Br shifts the equilibrium between dormant and propagating radical species toward

dormant species. As a result, the mixed halogen system R-Br/CuCl causes faster initiation, slower propagation, and therefore better control of molecular weight [87].

Based on these studies, it can be stated that SI-ATRP is an excellent method for synthesizing polymer brushes. ATRP is a highly adaptive and robust method, applicable to a wide range of monomers and functional groups, and at the same time able to tolerate relatively high levels of impurities. Especially, the consumption of residual traces of oxygen by redox mechanism makes ATRP insensitive to relatively low levels of oxygen impurity. Furthermore, using ATRP allows the option of commercially available catalyst systems and immobilizable initiators as a practical advantage.

However, it should be mentioned that SI-ATRP has also limitations. Controlled polymerization monomers that can react with the metal catalyst are particularly problematic. The ligand selection is also a crucial step in ATRP, open to problems. The use of multidentate amines, such as PMDETA or HMTETA, leads to fast polymerization rates, probably due to the formation of copper complexes with lower redox potentials compared to other ligand copper complexes such as 2,2′-bipyridine. Higher activation rate of dormant alkyl halides is a consequence of this lower redox potential. On the other hand, derivatives of bipyridine that have different solubility behavior are useful for water based systems and hydrophilic polymers [88].

Block copolymer synthesis by ATRP surves to two purposes: Confirming the livingness of the ATRP and creating tailored structures for special purposes.

Currently, there are no detailed studies, in the literature, on the amphiphilic block copolymers from the nanoparticle surface, via ATRP. Amphiphilic blocks grown from the surface of nanoparticles may bring not only enhanced stability and solubility, but also superior properties such as biocompatibility, stimuli responsiveness and potential bases for more complex hybrid structures. Therefore, PS, PMMA and PS-b-PHEMA and PS-b-PDMAEMA were grown from initiator (CPTMS/BPTMS) coated MNPs via ATRP (Figure 21).

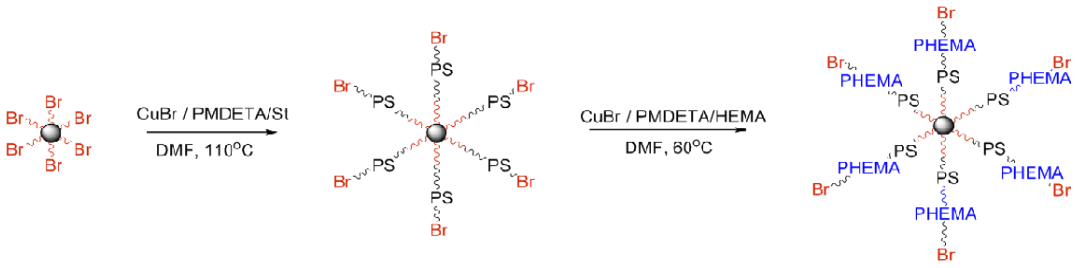

Figure 21. Typical scheme of polymerization from BPTMS coated MNPs

3.2 Experimental Section

3.2.1 Materials

All reagents were used as received unless indicated otherwise. CuCl, pentamethyl diethylenetriamine (PMDETA), styrene, xylene, CuBr, $CuBr_2$, methyl methacrylate (MMA) were purchased from Acros Organics. 2,2′-Bipyridine, 2-hydroxyethyl methacrylate (HEMA) and 2-Dimethylaminoethylmethacrylate (DMAEMA) were purchased from Aldrich. o-Dichlorobenzene (o-DCB) was purchased from Carlo Erba.

3.2.2 Growth of PS and PMMA Polymers from the Surface of MNPs

Initiator coated nanoparticles were used as a colloidal solution in DMF or xylene. In a typical preparation, initiator coated particles; catalyst (CuCl or CuBr), in some cases $CuBr_2$ and the monomer were first deoxygenated for 30 minutes in a Schlenk flask. Then, deoxygenated ligand (PMDETA or 2,2'-bipyridine) was injected to the reaction and polymerization was carried out at the desired temperature. The viscosity of the solution increased with time. At the desired polymerization time, polymerization solution was diluted with THF and precipitated into methanol.

The precipitated brown powder was dried in vacuum oven at 40 °C overnight. Dry polymer was dissolved again and passed through basic alumina column in order to remove copper from the system. Polymer was reprecipitated in methanol. Details of the polymerization conditions are given in Table 2 for PMMA and Table 3 for PS.

Table 2. Polymerization conditions for MMA polymerization from MNP surface

SAMPLE ID	Initiator/CuX/ PMDETA/monomer	Initiator	Transition Metal	Time (h)
SIMMA01	**1 : 1 : 1 : 100**	**CPTMS**	**CuCl**	**12**
SIMMA02	**1 : 1 : 1 : 100**	**BPTMS**	**CuCl**	**3**
SIMMA03	**1 : 1 : 1 : 100**	**BPTMS†**	**CuBr**	**3**

BPTMS† Initiator was synthesized via Ligand Exchange Method
*Polymerizations were carried out in DMF(V/V ratio 1/1) at 90 °C

Table 3. Polymerization conditions for PS polymerization from MNP surface

SAMPLE ID	Initiator/CuX/ PMDETA/monomer	Initiator	Transition Metal	Time (h)
SIPS01	**1 : 1 : 1 : 100**	**CPTMS**	**CuCl**	**12**
SIPS02	**1 : 1 : 1 : 100**	**BPTMS**	**CuCl**	**3**
SIPS03	**1 : 1 : 1 : 100**	**BPTMS†**	**CuBr**	**3**
SIPS04	**1 : 1.2 : 12 : 1200**	**BPTMS†**	**CuBr**	**45**
SIPS05	**1 : 1.2 : 12 : 1200**	**BPTMS†**	**CuCl**	**45**
SIPS06	**1 : 0.6[a] : 6 : 6 : 600**	**BPTMS†**	**CuBr/Cu(II)**	**14**
SIPS07	**0.1[b] : 1 : 6 : 6 : 600**	**BPTMS†**	**CuBr/F.I.**	**14**

BPTMS† Synthesized via Ligand Exchange Method
[a] $CuBr_2$
[b] Free initiator: EBIB
*Polymerizations were carried out in DMF(V/V ratio 1/1) at 110 °C

3.2.3 Growth of PS-b-PHEMA Polymer from the Surface of MNPs

30 mg of PS coated washed magnetic nanoparticles (macroinitiators) in 4 ml DMF, CuBr, $CuBr_2$ and 2 -hydroxyethyl methacrylate were first deoxygenated for 30 minutes. Then, deoxygenated ligand (PMDETA or 2,2-bipyridine dissolved in DMF) was injected to the reaction. The reaction was allowed to continue at 60°C for predetermined amount of time. The viscosity of the solution increased with time. After the polymerization was complete, the remaining solution was diluted with DMF and precipitated to petroleum ether. The precipitated powder was dried in

vacuum oven. Dry polymer was redissolved in DMF and passed through alumina column in order to remove copper from the system. PS-b-PHEMA chains were cleaved from the MNPs as described below.

Table 4. Polymerization conditions for PS-b-PHEMA growth from MNP surface

SAMPLE ID	Initiator/CuX/ PMDETA/monomer	Initiator	Transition Metal	Time (h)
PS-b-HEMA01	**1:1:1:300**	**CuBr/Cu(II)**	**PMDETA**	**24**
PS-b-HEMA02	**1:1:1:1200**	**CuBr/Cu(II)**	**PMDETA**	**72**
PS-b-HEMA03	**1:1:1:1200**	**CuBr/Cu(II)**	**Bipyridine**	**72**

*Polymerizations were carried out in DMF(V/V ratio 1/1) at 110 °C

3.2.3.1 Cleavage of polymers from the MNPs

Typically, 20 mg of the polymer-grafted MNPs were treated with 3 ml 10 % HF aqueous solution for 4 hours. The brown color of the MNP cannot be seen after the HF treatment. After being neutralized by NaOH, cleaved polymer chains were extracted with chloroform. Polymers were isolated after chloroform was evaporated by a rotaryevaporator. Polymers were redissolved in THF for molecular weight analysis by GPC.

3.2.4 Growth of PS-b-PDMAEMA Polymer from the Surface of MNPs

30 mg of PS coated washed particles (macroinitiators) in DMF, CuBr, $CuBr_2$ and dimethyl amino ethylmethacrylate (DMAEMA) were first deoxygenated for 30 minutes. Then, deoxygenated ligand (PMDETA or 2,2-bipyridine dissolved in DMF) was injected to the reaction. The reaction was allowed to continue at 60°C for predetermined amount of time. The viscosity of the solution increased with time. After the polymerization was complete, the remaining solution was diluted with DMF and precipitated to petroleum ether. The precipitated powder was dried in vacuum oven. Dry polymer was re-dissolved in DMF and passed through alumina column in order to remove copper from the system. PS-b-PDMAEMA chains were cleaved from the MNPs as described above.

Table 5. Polymerization conditions for PS-b-PDMAEMA growth from MNP surface

SAMPLE ID	Initiator/CuX/ Ligand/ Monomer	Initiator	Transition Metal	Ligand	Solvent	Time (h)
PS-b-PDMAEMA01	1:1:1:500	SIPS10	CuBr	PMDETA	DMF	72
PS-b-PDMAEMA02	1:1:1:500	SIPS12	CuCl	PMDETA	DMF	72
PS-b-PDMAEMA03	1:1:1:1000	SIPS11	CuCl	PMDETA	DMF	180
PS-b-PDMAEMA04	1:1:1:1000	SIPS11	CuCl	Bipyridine	DMF	180
PS-b-PDMAEMA05	1:1:1:1000	SIPS11	CuBr	Bipyridine	o-DCB	96
PS-b-PDMAEMA06	1:1:1:1000	SIPS13	CuBr	Bipyridine	o-DCB	120

*Polymerizations were carried out at 60 °C
Solvent/Monomer(V/V): 1:5

3.2.5 Characterization Methods

Hydrodynamic size of the particles were measured by Malvern ZetaS Dynamic Light Scattering unit and reported as the number based average. Chemical characterization of nanoparticles was done by FTIR. IR spectra of the nanoparticles were recorded on a Nicolet FTIR instruments using KBr pallet of the dried samples. Organic content of the nanoparticles and quantification of the initiators on the particles were determined by Thermogravimetric analyses (TGA). TGA was performed on a Seiko SSC 5200 TG/DTA under N_2 with 10°C/min heating rate. Polymer molecular weights were determined by Gel Permeation Chromothography (GPC). GPC analysis was done on a Agilent 1000 equipped with a refractive index detector, using THF as an eluent, at 25°C at 1mL/min flow rate. Molecular weights were estimated with PS standards. Thermal properties of polymers were analyzed by TA Q200 Differential Scanning Calorimeter. Glass transition temperatures were recorded based on the second heating run at 10°C/min rate after initial heat/quench cycle under nitrogen.

3.3 Results and Discussion

Because ATRP is a controlled polymerization method, polymer molecular weight (M_w) can be tailored by the monomer/initiator ratio and the reaction time. The amount of initiator attached to the particle was calculated from the weight loss of CPTMS coated MNP recorded on a TGA. Then, the number of moles of monomer needed for the targeted molecular weight was calculated from the number of moles of initiator. Moreover, in order to understand better kinetics of surface initiated polymerization reactions were performed in different conditions.

3.3.1 Growth of PMMA from the Surface of MNPs

PMMA was grown from the particle surface using initiator coated MNPs. Different polymerizations were performed by changing the conditions in order to achieve a high molecular weight PMMA. Polymerizations were initiated using both CPTMS which is a primary chlorinated initiator or BPTMS which is a tertiary brominated initiator.

Initiating MNPs were used either as suspensions in DMF or as dried powders. All the conditions are given in Table 6.

Table 6. Polymerization conditions for PMMA growth from MNP surface

SAMPLE ID	Initiator	Transition Metal	Solvent	Time (h)	Conv. (%)	Mw	Mwtheo	PDI
SIMMA01	**CPTMS**	**CuCl**	**DMF**	**12**	**60**	**187K**	**6K**	**1,4**
SIMMA02	**CPTMS**	**CuCl**	**DMF**	**12**	**100**	**-**	**-**	**-**
SIMMA03	**CPTMS**	**CuCl**	**DMF**	**3**	**100**	**-**	**-**	**-**
SIMMA04	**CPTMS**	**CuCl**	**Xylene**	**3**	**100**	**-**	**-**	**-**
SIMMA05	**BPTMS†**	**CuBr**	**DMF**	**3**	**-**	**-**	**-**	**-**

BPTMS† Synthesized via Ligand Exchange Method
Solvent/Monomer(V/V): 1:1
*All trials were carried out at 90 °C,with the ratio of 1:1:1:100

The resulting PMMA coated MNPs were compared in terms of hydrodynamic size, colloidal stability, molecular weight, MW distribution, monomer conversion and the initiator efficiency.

As seen in Table 6, all trials except SIMMA01 have undergone rapid gelation observed in the form of high conversions in short polymerization times. A major problem encountered, as stated earlier in Chapter 1, was batch to batch variance in the initiator quality obtained via one pot synthesis in DMF. Previous researches in the literature stated that the polymerization of methyl methacrylate via ATRP was more controllable in nonpolar solvents compared to polar solvents such as DMF. Therefore, subsequent trial, SIMMA04, was conducted in a nonpolar solvent, xylene, but no improvement was observed.

As reported by Werne et al., the predominant termination modes in MMA polymerization are interparticle or intraparticle, since MMA does not undergo to thermal polymerization. Additionally, chain termination in the radical polymerization of MMA is predominantly (>90%) via disproportionation [89]. This process would form some macromonomer chain ends that could further react in the polymerization to yield branched and cross-linked structures such as in our case.

Comparison of TGA results of CPTMS coated MNPs (produced by one pot synthesis method) and SIMMA01, has revealed a distinctive increase of 41% in the organic content.however compared to the GPC results indicate dramatically low initiator efficiency.

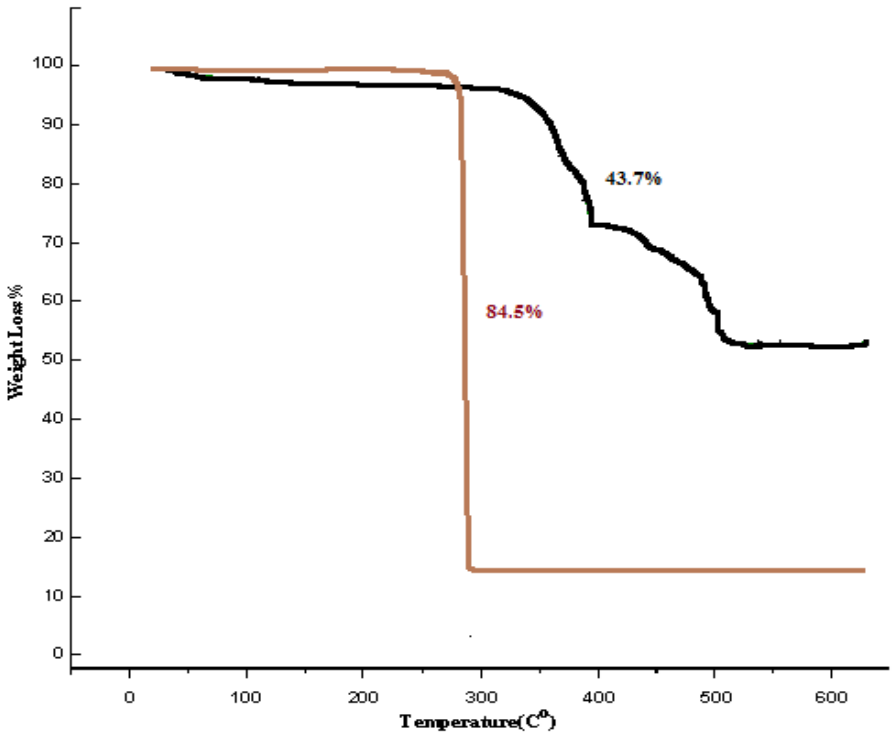

Figure 22. TGA of CPTMS coated MNPs(black) and SIMMA01(red)

Size distribution of PMMA coated particles measured by DLS, which were precipitated and suspended in DMF (SIMMA01) is shown in Figure 23. The average hydrodynamic size of CPTMS coated MNPs was about 90 nm. Afterwards the average size was increased to 200 nm. An increasing organic content and diameter indicates growth of polymer from the surface of the MNP.

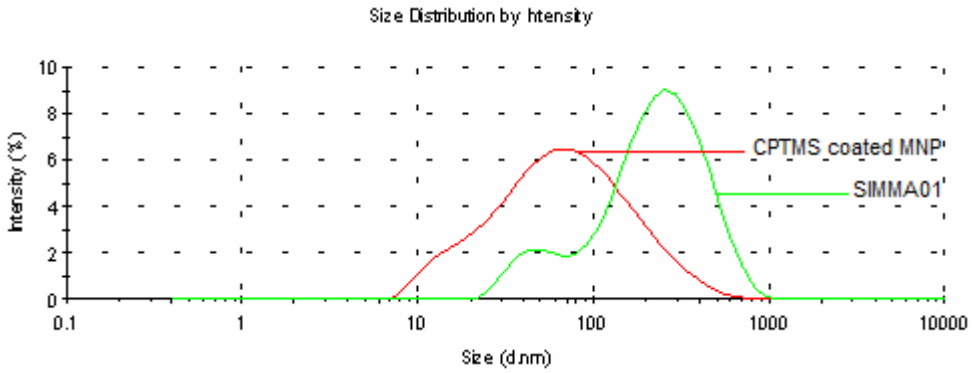

Figure 23. DLS measurement of CPTMS coated MNPs (red) and SIMMA01 (green)

3.3.2 Growth of PS from the Surface of MNPs

Styrene polymerizations were performed under different conditions using MNPs that are functionalized with different methods (Table 7). Due to batch to batch differences observed in one pot synthesis method, most of the polymerizations were initiated via MNPs functionalized via the ligand exchange method.

Table 7. Polymerization conditions (ATRP) for PS coated MNPs

SAMPLE ID	Initiator/CuX/ PMDETA/ monomer	Initiator	Transition Metal	Time (h)	Conv. (%)	Mw	Mwtheo	PDI
SIPS01	1 : 1 : 1 : 100	CPTMS	CuCl	12	100	-	10K	-
SIPS03	1 : 6 : 6 : 600	CPTMS†	CuBr	14	-	-	-	-
SIPS05	1 : 6 : 6 : 600	BPTMS†	CuBr	14	22	187K	13K	2,7
SIPS11	1 : 1.2 : 12 : 1200	BPTMS†	CuBr	45	65	254K	81K	2,7
SIPS12	1 : 1.2 : 12 : 1200	BPTMS†	CuCl	45	54	82K	67K	2,4
SIPS07	1 : 0.6 : 6 : 6 : 600	BPTMS†	CuBr/Cu(II)	14	20	170K	12K	2,5
SIPS08	0.1 : 1 : 6 : 6 : 600	BPTMS†	CuBr/F.I.	14	10	190K	6K	2,4

BPTMS† Synthesized via Ligand Exchange Method
*Polymerizations were carried out in DMF(V/V ratio 1/1) at 110 °C

PS coated MNPs were compared in terms of hydrodynamic size, colloidal stability, molecular weight, MW distribution, monomer conversion and the initiator efficiency. Monomer conversion (grams monomer used/grams of polymer obtained) increases with the reaction time. As foreseen**,** transition metal type affects the control and the rate of the reactions. As seen from the comparison of the trials SIPS11 and SIPS12, CuBr gives rise to a high polymerization speed while CuCl gives rise to relatively better controllability. Moreover, the use of CuCl together with BPTMS creater a mixed halide system that causes faster initiation, therefore better control of molecular weight, as reported also in the literature [87].

The experimental molecular weights were higher by a factor of 10, compared to the expected value and polydispersity values are far from controlled polymerization range. A possible explanation for this difference is that not all of the initiator sites on the nanoparticle surface initiated the growth of polymer chains, and this rationalization is consistent with the growing chains sterically blocking access of the catalyst to the neighboring initiation sites on the nanoparticle surface.

Two methods examined previously for inducing molecular weight control were the addition of deactivator and the addition of "sacrificial" free initiator to the polymerization system [84-85]. The purpose of adding free initiator to the polymerization medium was lowering the initial monomer-to-initiator ratio and increasing the overall initiator concentration, thereby allowing some radical coupling in solution to build up the concentration of deactivator. The addition of the $CuBr_2$ mitigated the insufficient formation of deactivator from the small initial concentrations of initiator and copper(I) catalyst. Both deactivator and free initiator additions have proven useful in controlling polymerization from the surface, in trials SIPS07 and SIPS08, respectively. As there is no significant difference from the reaction control perspective, we preferred deactivator addition in subsequent reactions, in order to get rid of the laborious purification step of the second method.

Measurement of the hydrodynamic sizes of the initiator coated MNPs and PS coated MNPs showed an increase in the hydrodynamic size with increasing monomer conversion. The hydrodynamic size of BPTMS coated MNPs prepared via ligand exchange were 6 nm (Figure 15) and after styrene polymerizations the average diameter increased up to 19 nm. As the conversion increase, the shell thickness, hence the size of the MNP should increase.

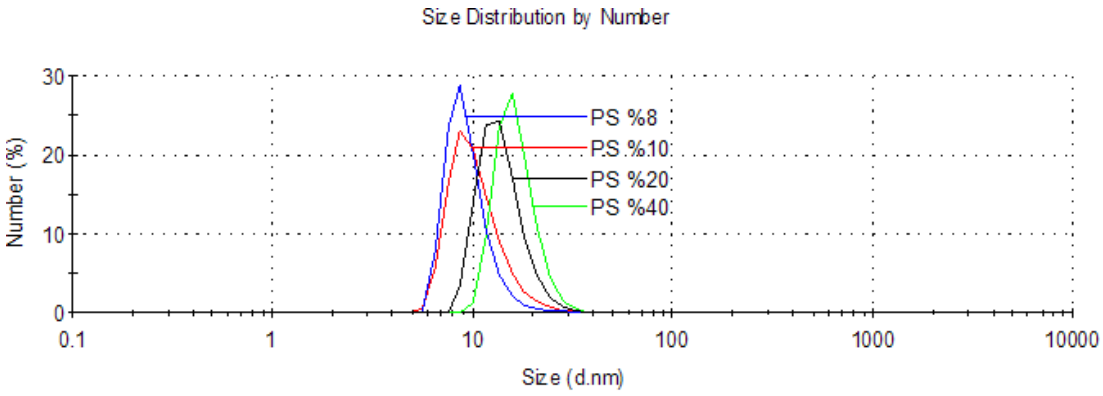

Figure 24. Hydrodynamic sizes of PS coated MNPs at different monmer conversions. All particles were washed and suspended in DMF

FTIR indicated the existance of the initiator moiety and the PS (Figure 25). Peaks at 3030-2800 cm^{-1} corresponds to aromatic C-H stretching vibrations of polystyrene. Peaks between 1500 to 2500 cm^{-1} the is characteristic for the monosubstituted benzene ring. Peaks at 1643 cm^{-1} and 1544 cm^{-1} corresponding to the N–C=O stretching and the large band around 1000 cm^{-1} corresponding to Si–O–Si vibrations indicates the existence of the BPTMS moiety on the magnetic nanoparticle. The Fe-O band at 601 cm^{-1} in BPTMS coated MNP spectra shifted to 540 cm^{-1} in PS coated MNP spectrum. The Fe-O band at 601 cm^{-1} in BPTMS coated MNP spectra shifted to 540 cm^{-1} in PS coated MNP spectrum.

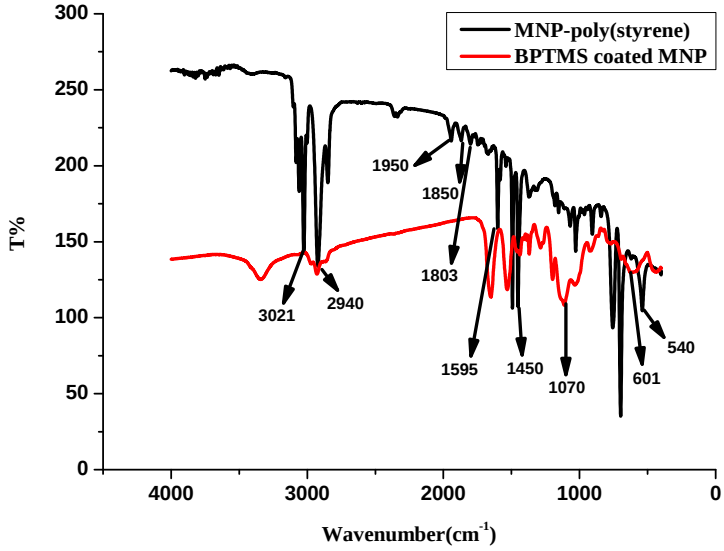

Figure 25. FT-IR spectrum of the BPTMS coated MNP and the PS synthesized from the same initiator

TGA plots of SIPS11 and BPTMS coated MNPs are shown in Figure 26. A weight loss of 7% is observed in the plot of SIPS11 shown in red, at about 100 °C, indicating that removal of the solvent from the system wasn't complete. Then, a major weight loss of 90% starts at about 400 °C for the decomposition of polystyrene. The weight loss of 5% seen at about 200 °C is attributed to the remaining lauric acid after the ligand exchange process and 23% at about 400 °C is caused by the decomposition of BPTMS. This data that, showing a weight loss of 67% caused by PS shell, is in accordance with the conversion of SIPS11 calculated from experimental results.

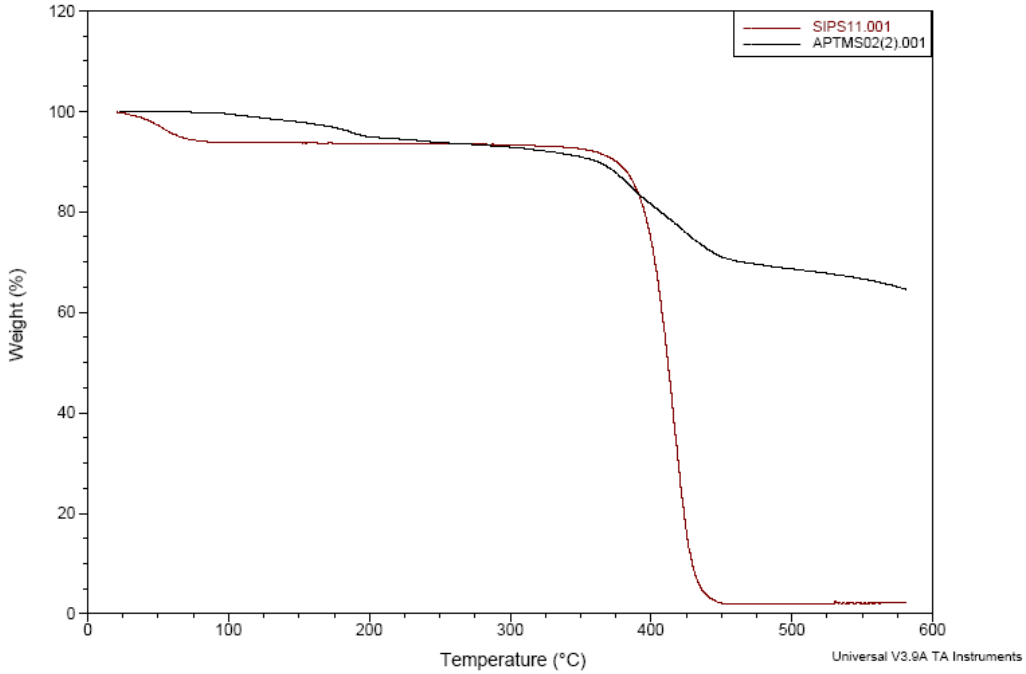

Figure 26. TGA of BPTMS coated MNP and PS coated MNP (SIPS11)

3.3.3 Growth of PS-b-PHEMA from the Surface of MNPs

Poly(styrene)-b-poly(hydroxyethyl methacrylate) amphihilic block copolymers were synthesized using SIPS07 as macroinitiator. Growth of hydrophilic PHEMA block of various molecular weights, on hydrophobic PS block at fixed molecular weight was targeted. All polymerizations were performed with 10% $CuBr_2$ using bipyridine or PMDEATA as a ligand in DMF. Details are in Table 8.

Bipyridine causes a faster reaction with HEMA as reported in the literature but PMDETA also works. The former gives about 83% conversion in 72 h whereas the later hits only 33% under the identical conditions. As expected, with increasing conversions solubility behavior of polymers were dramatically changed. Due to increasing tendency to hydrophilicity, while PHEMA01 was soluble in THF, PHEMA03 that has longer hydrophilic chain, was poorly soluble in THF.

Table 8. Polymerization conditions (ATRP) for PS-b-PHEMA

SAMPLE ID	Initiator/CuX/ Ligand/ monomer	Transition Metal	Ligand	Time (h)	Conv. (%)
PS-b-PHEMA01	**1:1:1:300**	**CuBr/Cu(II)**	**PMDETA**	**24**	**5%**
PS-b-PHEMA02	**1:1:1:1200**	**CuBr/Cu(II)**	**PMDETA**	**72**	**33%**
PS-b-PHEMA03	**1:1:1:1200**	**CuBr/Cu(II)**	**Bipyridine**	**72**	**83%**

*$CuBr_2$ added at a ratio of 1/10 relative to CuBr
*SIPS7 used as initiator
*Polymerizations were carried out in DMF(V/V ratio 2/1) at 60 °C

The increase in particle size is evidently seen in DLS measurements. After HEMA polymerizations the hydrodynamic sizes of MNPs were increased to 20 nm while the average hydrodynamic size of PS coated MNPs used as macroinitiator were 12 nm.

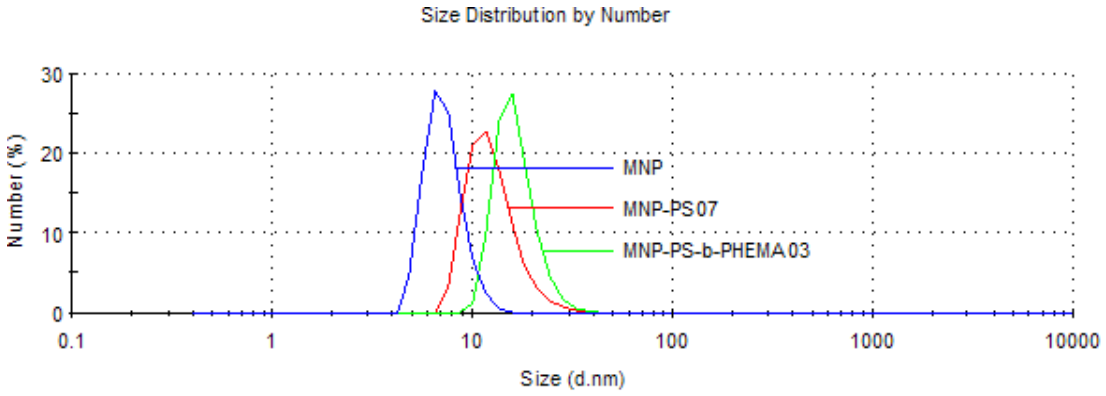

Figure 27. Hydrodynamic sizes of BPTMS coated MNPs (blue), MNP-PS07 (red) and MNP-PS-b-PHEMA03(green) in DMF

The formation of PS-b-PHEMA copolymers is evident from the observed C=O stretching band at 1716 cm^{-1} and O-H stretching at 3556 cm^{-1} in the FTIR spectrum. Furthermore the peak at 3000 cm^{-1} which overlaps with the peaks of macroinitiator, belongs to aromatic C-H stretching bands of polystyrene.

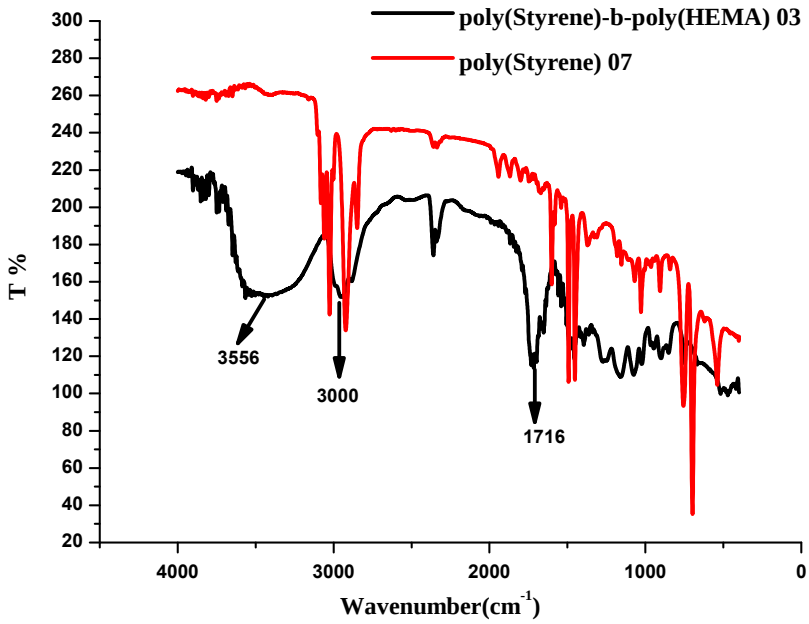

Figure 28. FT-IR spectrum of SIPS07 (red) and SIPS-bPHEMA03(black) coated MNP

3.3.4 Growth of PS-b-PDMAEMA Polymer from the Surface of MNPs

Poly(styrene)-b-poly(dimethyl amino ethyl methacrylate) amphiphilic copolymers were synthesized using PS coated MNPs as macroinitiator. Until now, there have been only a few studies relating to PS-b-PDMAEMA blocks [90]. As seen in Table 9, ligand and solvent choice affects the rate of polymerization tremendously. Among all the trials, best results were obtained from the combination of tertiary bromide initiator, bipyridine ligand and o-DCB solvent.

Table 9. Polymerization conditions (ATRP) for PS-b-PDMAEMA

SAMPLE ID	Initiator/CuX/ Ligand/monomer	Initiator	Transition Metal	Ligand	Solvent	Time (h)	Conv. (%)	PDI	Mw
PS-b-PDMAEMA01	**1:1:1:500**	**SIPS10**	**CuBr**	**PMDETA**	**DMF**	**72**	**3%**	**-**	**-**
PS-b-PDMAEMA02	**1:1:1:500**	**SIPS12**	**CuCl**	**PMDETA**	**DMF**	**72**	**3%**	**2,2**	**81K**
PS-b-PDMAEMA03	**1:1:1:1000**	**SIPS11**	**CuCl**	**PMDETA**	**DMF**	**180**	**5%**	**2,4**	**208K**
PS-b-PDMAEMA04	**1:1:1:1000**	**SIPS11**	**CuCl**	**Bipyridine**	**DMF**	**180**	**none**	**N/A**	**N/A**
PS-b-PDMAEMA05	**1:1:1:1000**	**SIPS11**	**CuBr**	**Bipyridine**	**o-DCB**	**96**	**15%**	**2,4**	**66K**
PS-b-PDMAEMA06	**1:1:1:1000**	**SIPS13**	**CuBr**	**Bipyridine**	**o-DCB**	**120**	**20%**	**2,1**	**181K**

*Polymerizations were carried out at 60 °C
Solvent/Monomer(V/V): 1:5

DLS measurements were performed in order to observe the hydrodynamic sizes of MNPs after homo and block copolymerizations. While the increase isn't so dramatic, it's clearly visible that the hydrodynamic particle size that is 12 nm before the block copolymerization becomes 20 nm (Figure 29).

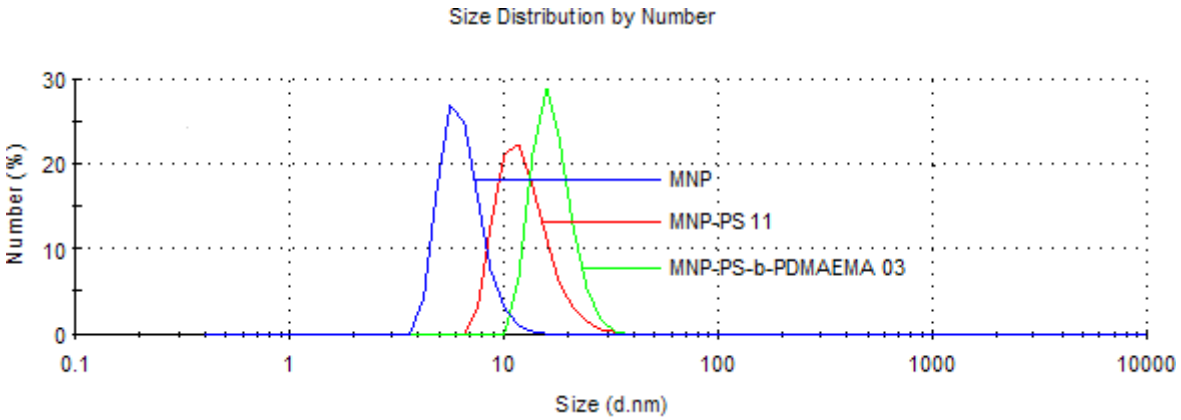

Figure 29. Hydrodynamic sizes of BPTMS coated MNPs (blue), MNP-PS11 (red) and MNP-PS11-b-PDMAEMA03(green) in DMF

In Figure 30, red line represents the FT-IR spectrum of PS coated MNPs and the black line represents PS11-b-PDMAEMA03 coated MNPs. Aromatic C-H stretching vibrations at 3021 and 2780 cm^{-1}, multiple bands between 1500 and 2000 cm^{-1}, typical C-to-C aromatic stretching at 1400 cm^{-1} and 1600 cm^{-1} indicates the presence of PS in PS11-b-PDMAEMA03 coated MNPs. The sharp carbonyl stretching band at 1710 cm^{-1} and C-N stretching at 1150 cm^{-1} indicates the presence of PDMAEMA.

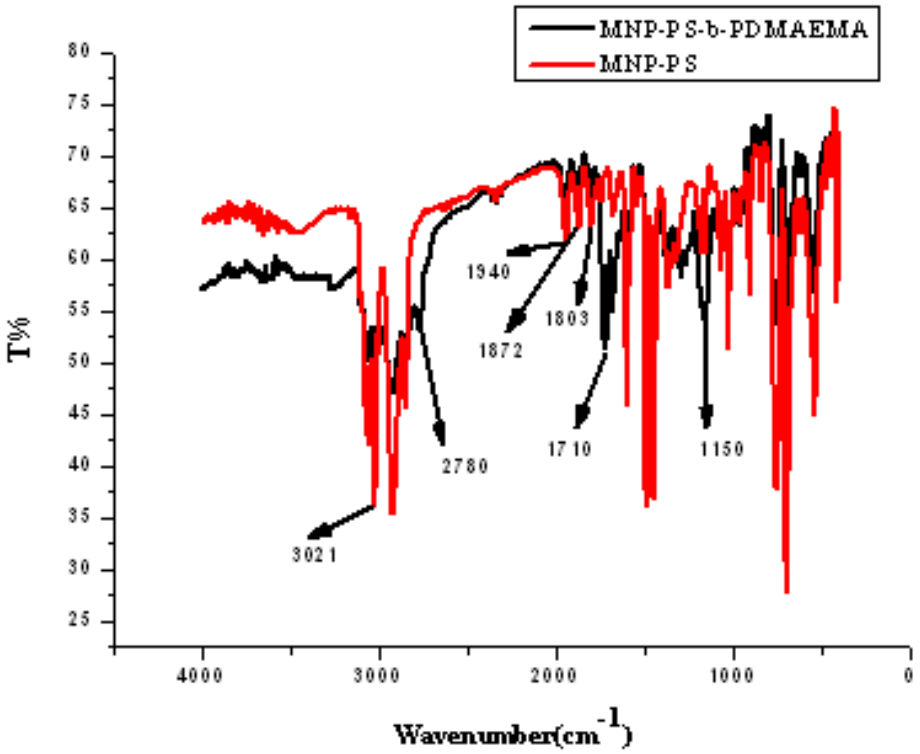

Figure 30. FT-IR spectrum of PS (red) and PS-b-PDMAEMA(black) coated MNP

Another method used for the characterization of block polymers was Differential Scanning Calorimetry. As seen in the Figure 31, thermogram of PS11-b-PDMAEMA03 claved from nanoparticle surface, shows two glass transition temperatures (T_g) at 80 ºC and 112 ºC. The one at 80 ºC, corresponds to the T_g of poly(styrene) and the one at 112ºC corresponds to the Tg of poly(dimethyl amino ethyl methacrylate), the latter being confirmed by coinciding with the Tg of poly(dimethyl amino ethyl methacrylate) homopolymer synthesized separately for comparison [91].

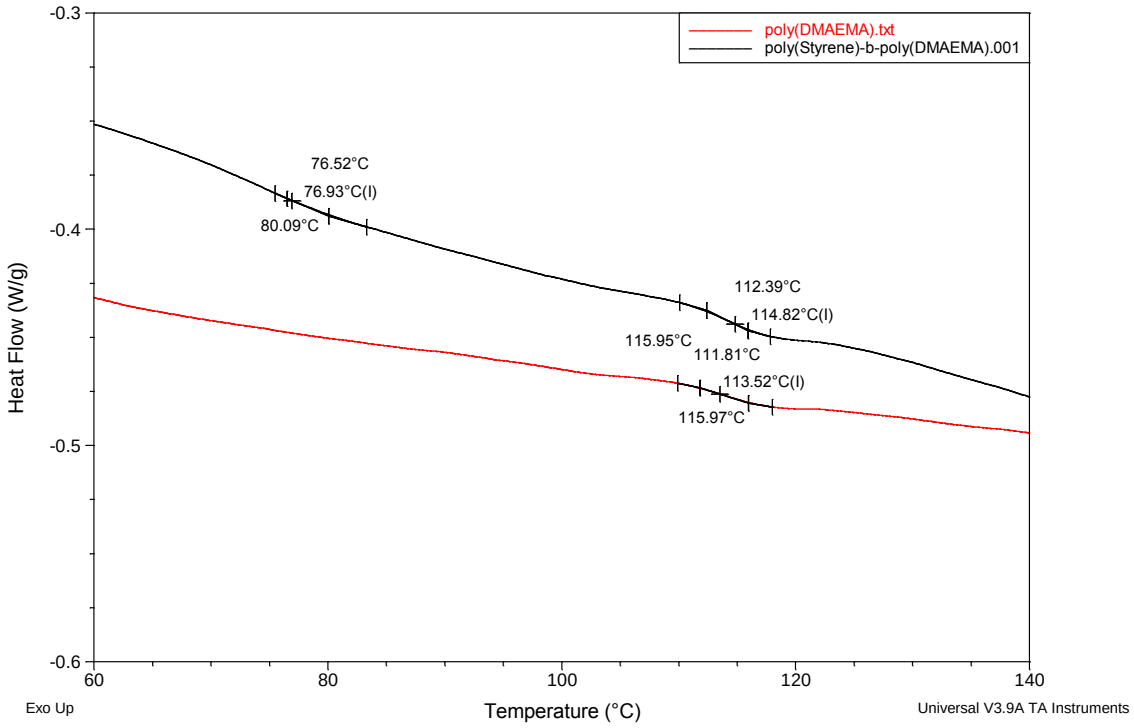

Figure 31. DSC plot of PS11-b-PDMAEMA03 (red) and PDMAEMA (black)

Thermal Gravimetric Analysis was also performed for PS coated MNPS used as a macroinitiator and PS12-b-PDMAEMA02 coated MNPs (Figure 32). Weight losses matches with the conversion calculated from experimental results. The minor weight loss of 3% that starts at 320 ºC indicates the decomposition of PDMAEMA02. The major weight loss of 82% that starts at 400 ºC indicates the decomposition of PS.

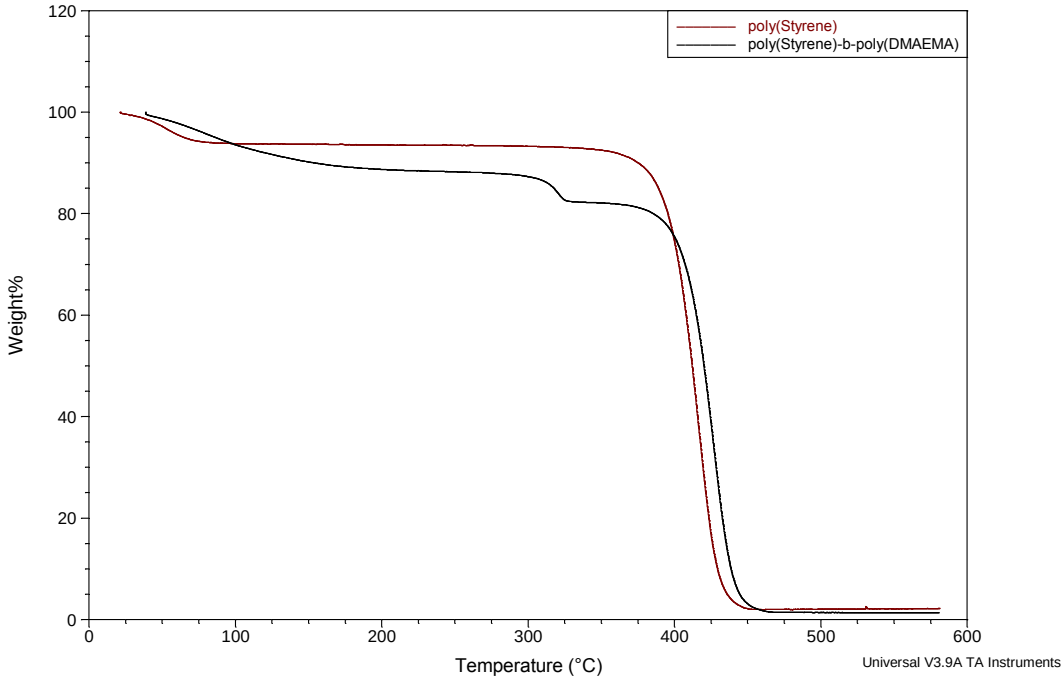

Figure 32. TGA of PS coated MNP(SIPS12) and PS12-b-PDMAEMA02 coated MNP

Molecular weights were measured from the cleaved polymer chains. The increase in molecular weight is seen also by GPC measurement. PS macroinitiator used had a M_w of 135K, yet the block copolymer had a Mw of 181K. This was obtained at 20 % conversion.

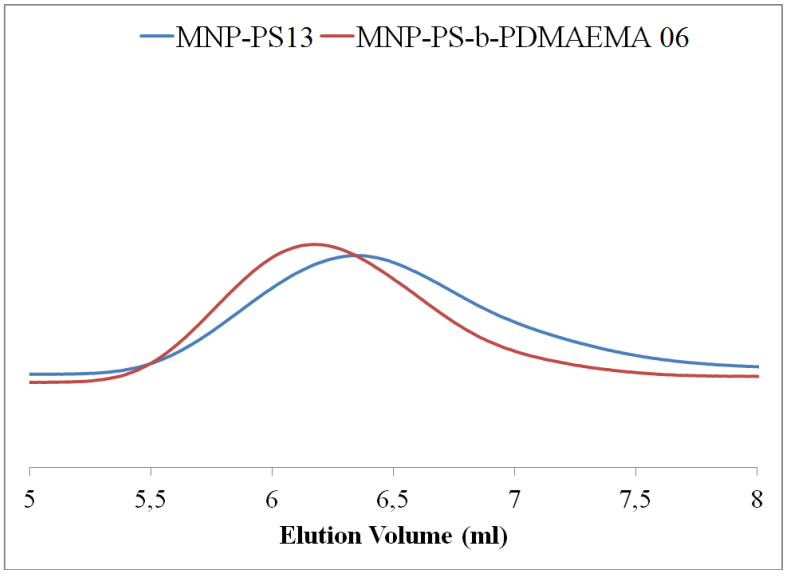

Figure 33. GPC data plot of PS13 coated MNP and PS-b-PDMAEMA06 coated MNP

3.4 Conclusion

In this chapter, details of surface initiated polymerization via ATRP were discussed. Most importantly, the effects of changes in reaction parameters were studied. All trials resulted in polydispersity values higher than those expected for controlled polymerization. High polydispersities, together with the molecular weights that are higher than theoretical values point to low initiator efficiency as reported also in the literature.

However, the brown color of the polymers indicate that the polymerization from the surface of MNPs. Moreover, mononodal peaks of GPC traces prove that the polymerization occurs only from the surface of nanoparticles. Furthermore, the size increase in DLS and GPC, while not dramatic, indicates polymer chains have living character and retain the ability to undergo block copolymerization. GPC measurements could not be performed for PHEMA blocks since the samples were insoluble in THF; but the solubility change towards hydrophilicity and the increase in conversions are the signs of block copolymerization.

In conclusion, despite various drawbacks, PS-b-PDMAEMA and PS-b-PHEMA polymerizations were accomplished from MNP surfaces. These amphiphilic block copolymers are not only stimuli responsive coatings on nanoparticle surfaces, but also the structures that will function as a bridge between two nanoparticles.

Chapter 4 Quantum Dots

4.1 Introduction

Quantum dots are of great interest due to their potential applications in light emitting diodes, lasers, solar cells and biological labeling. These applications are mainly based on their unique photoluminescence characteristics such as long-term photostability, high quantum yield (QY), narrow and size dependent spectral bandwidth.

Recently, inorganic/organic hybrid materials that combine the unique properties of quantum dots with that of polymers have become a hot topic. Polymers can be thought as versatile surface modifiers with numerous functional groups. Polymers can provide various properties such as solubility in different solvents, stability and film formation. Additionally, sophisticated properties such as a reversible stimuli-responsive behavior (*e.g.*, pH/T responsiveness) are possible. Moreover, surface functionalization with polymers allows the direct linkage of further substrates providing more complex structures.

Generally, polymer chains can be introduced by two methods. One is a polymerization from the nanoparticle surface, namely grafting-from approach. For this purpose, an initiator like a radical or ROMP starter, a dithioester for RAFT polymerization, or a halogen-containing surfactant for ATRP has to be linked to the particle surface [92-94].

As an alternative approach, it is also possible to anchor premade polymers containing anchor groups at the chain ends or an anchor block by simple ligand exchange [95-96]. However, they usually suffer from drawbacks such as dramatic reduction in the quantum efficiency, colloidal stability, or an increase in the overall hydrodynamic size.

In the past, most of the studies aiming to modify QD surfaces involved replacing TOPO with another monodentate ligand [97]. Recently, polydentate ligands have attracted great interest since they provide enhanced coordination interactions and extraordinary stability due to their multiple binding sites. Conventional homopolymers can be thought of as multidentate ligands if a suitable functionality can be introduced as a pendant group in the repeat unit. Previously our group have reported the direct synthesis of CdS nanoparticles coated with poly(acrylic acid)(PAA) and investigated the influence of PAA molecular weight on the size and quantum

yield [98]. The direct synthesis turned out to be a straightforward, mild and easy way to produce stable and highly luminescent QDs.

PDMAEMA has recently been a focus of interest, being a T/pH responsive smart polyelectrolyte. Due to the tertiary amine groups, PDMAEMA is known to have LCST, which means that its solubility behavior change over a critical temperature, introducing responsiveness to external stimuli such as pH and temperature change. Moreover, this smart polyelectrolyte is soluble both in water and in organic solvents such as DMF, dioxin, dichloromethane, acetone.

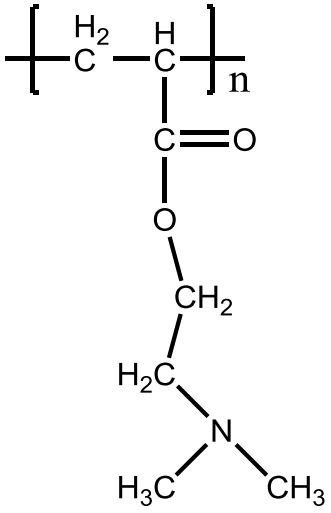

Figure 34. Poly(dimethylamino ethyl methacrylate)(PDMAEMA)

Recently there have been few studies reporting PDMAEMA stabilized quantum dots. Most of them are synthesized either via ligand exchange method or via surface initiated polymerization [99-102]. Only very recently, Basu et al. synthesized CdS nanoparticles directly in poly(styrene-*b*-2-(N,N-dimethylamino)ethyl methacrylate) diblock copolymers micelles, but no other study on in situ coating with PDMAEMA or detailed study on PDMAEMA coated QDs found in the literature [103]. However, none of these studies provide a detailed analysis of the mechanism and stimuli responsiveness of these smart hybrid nanoparticles. In this chapter, we present the detailed analysis of PDMAEMA coated CdS synthesized via a novel, straightforward route. In this context, effects of pH, T, ligand amount on particle size and luminescence behavior and the reversible stimuli responsive character were investigated.

4.2 Experimental

4.2.1 Materials

All chemicals were analytical grade or of the highest purity available. Sodium sulfide trihydrate ($Na_2S.3H_2O$), cadmium acetatedihydrate ($Cd(Ac)_2{\cdot}2H_2O$), Rhodamine B and HNO_3 (65 %) were purchased from Merck. DMAEMA and AIBN(2,2'-azo bis(isobutyronitrile) were purchased from Sigma Aldrich. Sodium hydroxide was purchased from Aldrich. Only double distilled Milli-Q water (Millipore) was used as the solvent. JEFFAMINE (XTJ-501) and ED2003 were received from Huntsman Co as a gift.

4.3 Synthesis of CdS stabilized with PDMAEMA

4.3.1 Multidentate Ligand Synthesis

4.3.1.1 Free Radical Polymerization of Monomers (FRP)

The appropriate amounts of solvent, monomer and initiator (AIBN) were added in a small round-bottomed flask (usually 10 or 25 ml). This solution was deoxygenated for 20 minutes and immersed in an oil bath at a predetermined temperature. The reaction conditions are listed in Table 10.

Table 10. Polymerization Conditions of Multidentate Ligands

SAMPLE ID	Initiator:monomer	Initiator	Monomer Concentration	Temp. (°C)	Time (h)
PHEMA01	**1:330**	**AIBN**	**3M**	**50**	**4**
PHEMA05	**1:330**	**AIBN**	**3M**	**50**	**2**
PNIPA01	**1:100**	**AIBN**	**2,2M**	**50**	**24**
PDMAEMA01	**1:100**	**AIBN**	**3M**	**60**	**24**
PDMAEMA08	**1:100**	**AIBN**	**3M**	**60**	**24**

All reactions were performed in DMF

4.3.1.2 ATRP of Monomers

In a typical preparation, CuBr, solvent and the monomer were first deoxygenated for 30 minutes in a Schlenk flask. Then, deoxygenated 2,2´-bipyridine was injected to the reaction. Finally, deoxygenated EBIB was injected to the reaction and polymerization was carried out at the desired temperature. After the polymerization was complete, the remaining solution was diluted with DMF and precipitated in petroleum ether. The precipitated powder was dried in a vacuum oven. Dry polymer was re-dissolved in DMF and passed through an alumina column in order to remove copper from the system. Finally, the solution was precipitated in hot water and dried in a lyophilizer. The reaction conditions are listed in Table 11.

Table 11. Polymerization Conditions of DMAEMA

SAMPLE ID	Initiator/CuX/Bpy/monomer	Transition Metal	Temp. (°C)	Time(h)
PDMAEMA05	**1:1:2:300**	**CuBr**	**60**	**4**
PDMAEMA06	**1:1:2:300**	**CuBr**	**60**	**6**
PDMAEMA07	**1:1:2:300**	**CuBr**	**60**	**22**

*All reactions were performed in o-DCB

4.3.2 Synthesis of CdS nanocrystals

Preparation of Cd^{2+} solution

In a typical synthesis, 66,63 mg ($2{,}5.10^{-4}$ mol) $Cd(Ac)_2{\cdot}2H_2O$ was dissolved in 50 ml deionized water and added to 250ml three-necked round bottomed flask fitted with a mechanical stirrer. Appropriate amount of ligand was calculated based on the desired ratio. For reactions run at pH 7.5, pH was adjusted with 10 M NaOH and/or 10 M HNO_3. This solution was deoxygenated for 15 minutes, and brought in an oil bath at 60°C.

Preparation of S^{2-} solution

13.2 mg $Na_2S{\cdot}3H_2O$ was dissolved in 50 ml deionized water in an ultrasonic bath and transferred into an addition funnel and deoxygenated for 15 min.

Preparation of CdS nanoparticles:

Sodium sulfide solution was added to the cadmium acetate solution drop by drop. After the addition was completed, reaction was stirred under nitrogen at set temperature for additional one hour. No further pH adjustment was done before UV-Vis or PL measurements. All ratios are listed in Table 12.

Table 12. Reaction Condition of CdS Synthesis

Sample ID	Ligand Type	Ligand/Cd	Cd/S	pH	Temp. (°C)	Solvent
CDS07	LAURICAC	2,5	2,5	-	60	Water
CDS08	SDS	2,5	2,5	7,5	60	Water
CDS04	HEMA monomer	2	2,5	7,5	RT	Water
CDS01	PEG 35000	2	2,5	7,5	60	Water
CDS05	JEFFAMINE 900	4	2,5	7,5	60	Water
CDS06	JEFFAMINE 2000	4	2,5	7,5	60	Water
CDS02	PHEMA01	2	2,5	7,5	60	Water
CDS03	PHEMA05	2,5	2,5	7,5	60	Water
CDS10	PNIPA01	2,5	2,5	7,3	RT	Water
CDS11	PNIPA01	4	2,5	7,3	RT	Water
CDS09	PDMAEMA 65K	2,5	2,5	7,5	60	Water
CDS12	PDMAEMA 65K	4	2,5	7,5	60	Water
CDS13	PDMAEMA 65K	1,5	2,5	7,5	60	Water
CDS14	PDMAEMA 65K	4	2,5	5	60	Water
CDS15	PDMAEMA 65K	4	2,5	7,5	90	Water
CDS16	PDMAEMA 65K	4	2,5	10	60	Water
CDS18	PDMAEMA 57K	6	2,5	8,3	60	Water
CDS19	PDMAEMA 57K	12	2,5	8,3	60	Water
CDS20	PDMAEMA 57K	12	2,5	7,5	RT	water
CDS21	PDMAEMA 57K	12	2,5	8,3	RT	water
CDS22	PDMAEMA 57K	6	2,5	8,3	RT	water
CDS23	PDMAEMA 57K	6	2,5	8,3	60	water
CDS24	PDMAEMA 57K	12	2,5	7,5	60	water
CDS25	PDMAEMA 57K	12	2,5	8,3	60	DMF
CDS26	PDMAEMA 57K	6	2,5	8,3	60	water

JEFFAMINE XTJ-501: Amine ended poly(ethylene oxide), M_w: 900g/mol
ED2003: Amine ended poly(ethylene oxide), M_w: 2000g/mol

4.3.3 Characterization Methods

Polymer molecular weights were determined by Gel Permeation Chromothography (GPC). GPC analysis was done on an Agilent GPC with Mixed-C column using THF as an eluent, refrective index detector and PS standards at flow rate of 1ml/min. DLS Hydrodynamic size of the particles were measured by Malvern ZetaS Dynamic Light Scattering unit Absorption spectra were recorded with a Schimadzu UV-Vis-NIR spectrophotometer model 3101 PC in the 300-600 nm range. Absorption of samples at the excitation wavelength was kept in the 15 % range by diluting the samples with water. Size of the CdS nanoparticles was calculated by using Brus Equation [19]. For the evaluation of photoluminescence and calculation of quantum efficiencies, samples were excited at the wavelength of 355 nm.

4.4 Results and Discussion

4.4.1 Polymer Synthesis

4.4.1.1 Synthesis Via Free Radical Polymerization (FRP)

Encouraged from few studies on the stabilization of quantum dots with polymeric ligands via ligand exchange, polymers of hydroxyethyl methacrylate, N-isopropyl acrylamide and dimethylamino ethylmethacrylate were synthesized via Free Radical Polymerization (Table 13) in order to be used as multidentate ligands in the synthesis of CdS nanocrystals [100-102]. All polymerizations were performed at 2-3M monomer concentration using AIBN initiator at 0.3-1.0 mol%. Polymerizations were ended at different times providing conversions between 38-85%.

Table 13. Free radical polymerization conditions of various monomers

SAMPLE ID	Initiator:monomer (mol:mol)	Initiator	Monomer Concentration (M)	Temp. (°C)	Time (h)	Conversion (%)
PHEMA01	**1:330**	**AIBN**	**3,0**	**50**	**4**	**65**
PHEMA05	**1:330**	**AIBN**	**3,0**	**50**	**2**	**38**
PNIPA01	**1:100**	**AIBN**	**2,2**	**50**	**24**	**80**
PDMAEMA01	**1:100**	**AIBN**	**3,0**	**60**	**24**	**85**

4.4.1.2 Synthesis Via ATRP

FRP leads to polymers with high molecular weights at very low conversion and they remain approximately at the same level throughout the reaction. In order to obtain ligands with different molecular weights and lower polydispersity, polymers of dimethylamino ethylmethacrylate were synthesized via conventional ATRP using EBIB initiator, CuBr catalyst and bipyridine ligand. Polymerizations were terminated at different time intervals. All PDMAEMAs had a PDI between 1.3-1.6 and had different Mw varying between 26,59K and 44,99K.

Table 14. Polymerization conditions for Multidentate Ligands*

SAMPLE ID	Initiator/CuBr/ Bpy/monomer	Temp. (°C)	Time (h)	Conversion (%)	Mw (g/mol)	PDI
PDMAEMA05	**1:1:2:300**	**60**	**4**	**65**	**32376**	**1,6**
PDMAEMA06	**1:1:2:300**	**60**	**6**	**69.5**	**37471**	**1,4**
PDMAEMA07	**1:1:2:300**	**60**	**22**	**97**	**44993**	**1,5**
PDMAEMA10	**1:1:2:300**	**60**	**2**	**50**	**26590**	**1,3**

*All reactions were performed in o-DCB

4.4.2 Synthesis of CdS Quantum dots

Synthesis of CdS with the in situ coating of the crystal was studied using different ligands as listed in Table 12. Lauric acid (LA) and sodium dodecylsulfate (SDS) coatings were tried with the idea of a ligand exchange after the synthesis. Namely, LA or SDS would have been exchanged with an appropriate polymer after the synthesis, yet, these fatty acids did not produce a luminescent QD. Both trials resulted in bulk products. LA result might be attributed to low solubility of LA in water. HEMA monomer was also tried as a coating ligand for CdS. If hydroxyls could bind to the cadmiums on the surface, stabilization could have taken place, resulting in a monomer coated CdS quantum dot. Such nanoparticles can take part in polymerization after the synthesis and get cooperated in different types of polymers. However, hydroxyl groups were not effective stabilizers and therefore Poly(HEMA) failed to stabilize QDs, as well. PEG and Jeffamines are used to evaluate ethylene oxide units as QD stabilizers yet, they have failed as a coating material and only bulk CdS was produced. PNIPA and PDMAEMA are the amide and tertiary amine, respectively, containing polymers that

were investigated as a coating for the QD in this thesis work. Although PNIPA bound QDs formed through S-S bond formation or through interdigitating functional PNIPA are reported in the literature, direct coating with PNIPA was not known.[104,105] Trials of this work indicated that amide units of NIPA cannot stabilize QDs. PDMAEMA on the other hand produced stable aqueous QDs with significant luminescence quality.

After the establishment that direct use of PDMAEMA works well for the stabilization of CdS nanoparticles, several trials were carried out changing reaction parameters in order to determine the factors influencing the optical and colloidal properties and to determine the best conditions to produce QDs emitting in different colors and having high quantum yield. Factors investigated are the ligand (PDMAEMA)/cadmium ratio, pH, reaction temperature and the polymer molecular weight. All QDs had a positive zeta potential indicating a positive surface that will support colloidal stability.

Reactions CDS09, CDS12 and CDS13 have shown that as ligand/Cd ratio increases, sizes of quantum dots get smaller indicated by a blue shift in the absorption onset in the UV-Vis absorption spectrum (Figure 36 and Table 15).

Based on the results obtained from reactions CDS26 and CDS23 which have used PDMAEMA of 32 K and 65 K, respectively, it can be concluded that the particle size increases with the increasing molecular weight. This observation is in agreement with our findings obtained from PAA coated QDs [98]. Interparticle bridging and larger globular size are effective in such results.

Study of the pH and temperature is rather complicated with PDMAEMA. PDMAEMA displays a lower critical solution temperature (LCST), meaning that the polymer becomes insoluble in water when solution temperature is raised to T>LCST. In case of PDMAEMA, which bears tertiary amine groups, LCST is affected by the pH.

Polymers were precipitated in reactions CDS15 and CDS16. At pH 7,5, the reaction couldn't be carried out at 90ºC since this temperature is above the LCST of PDMAEMA. The same phenomena occurred when the reaction was performed at pH 10 and at the room temperature. As the pH increases the LCST value decreases.

Yet, at pH 8,3 effect of the reaction temperature was studied successfully. As reactions CDS19 and CDS21 indicates the reaction temperature has a dramatic effect on the size of

quantum dots. QDs synthesized at 60 ºC emit blue whereas those synthesized at room temperature emit green light. This might be due to the temperature responsive character of PDMAEMA. As it is confirmed by DLS results, polymer chains tend to shrink and the hydrodynamic size of polymers tend to decrease with increasing temperature. So the synthesis at higher temperature may lead to nanoparticles with smaller size and blue luminescence.

The effect of variation in pH was studied at 60°C successfully. According to the results of reactions CDS19 and CDS25, increase in pH leads to smaller particle size and higher quantum yield. Furthermore, CDS14 conducted at pH 5 resulted in bulk CdS, despite the fact that PDMAEMA is soluble at these pH and temperature values. A plausible explanation is the protonation of tertiary amine end groups of PDMAEMA at low pH values. As expected, the protonation of amine sites increases hydrophilicity of polymer as seen also from the resistance to precipitation. Therefore, at low pH values the LCST of PDMAEMA increases dramatically, up to 90 ºC from its normal value of 60 ºC at pH 7,5. This fact is crucial since CdS nanoparticles interact with the free electron pair of amine end group. So, at low pH values the interaction between the ligand (PDMAEMA) and CdS nanoparticles decreases dramatically, leading to bulk material. In contrast, at high pH values such as 10, as seen in trial CDS15, the synthesis fails again but this time due to the rapid precipitation of PDMAEMA . Again, at these pH values, LCST of PDMAEMA was measured as 30 ºC, so it’s a consistent result since CDS15 was conducted at 60 ºC which is a higher temperature than LCST in that pH range.

Another fascinating result of this study is the unproblematic synthesis of quantum dots both in water and organic solvent such as DMF, as demonstrated in trials CDS25 and CDS19. Both trials resulted in approximately the same quantum yield and the same particle size. Moreover, interestingly, the quantum yield of CDS19 increased significantly after washing procedure. The washing procedure eliminates excess PDMAEMA resulting in this increased quantum yield.

Table 15. Reaction Condition of CdS Synthesis

SAMPLE ID	Ligand Type	Ligand/Cd	Cd/S	pH	T	Solvent	QY	Zeta Potential	Size	Band Gap (eV)	Result
CDS09	PDMAEM 65K	2,5	2,5	7,5	60	Water	6	-	3,9	2,64	YELLOW
CDS12	PDMAEM 65K	4	2,5	7,5	60	Water	23	-	2,7	3,03	BLUE/GREEN
CDS13	PDMAEM 65K	1,5	2,5	7,5	60	Water	5	-	4.1	2.61	WEAK YELLOW
CDS14	PDMAEM 65K	4	2,5	5	60	Water	-	-	-	-	No luminescence
CDS15	PDMAEM 65K	4	2,5	7,5	90	Water	-	-	-	-	Precipitated
CDS16	PDMAEM 65K	4	2,5	10	60	Water	-	-	-	-	Precipitated
CDS19	PDMAEM 57K	12	2,5	8,3	60	Water	17 (w:24)	42	2,7	3,03	BLUE
CDS20	PDMAEM 57K	12	2,5	7,5	RT	Water	10	7	3,5	2,73	YELLOW
CDS21	PDMAEM 57K	12	2,5	8,3	RT	Water	12	32	2,8	2,98	GREEN
CDS23	PDMAEM 57K	6	2,5	8,3	60	Water	8	48	3,5	2,74	YELLOW
CDS24	PDMAEM 57K	12	2,5	7,5	60	Water	12	53	3,3	2,78	GREEN
CDS25	PDMAEM 57K	12	2,5	8,3	60	DMF	15	13	2,7	3,03	BLUE/GREEN
CDS26	PDMAEM 32K	6	2,5	8,3	60	Water	5	28	3,1	2,85	GREEN

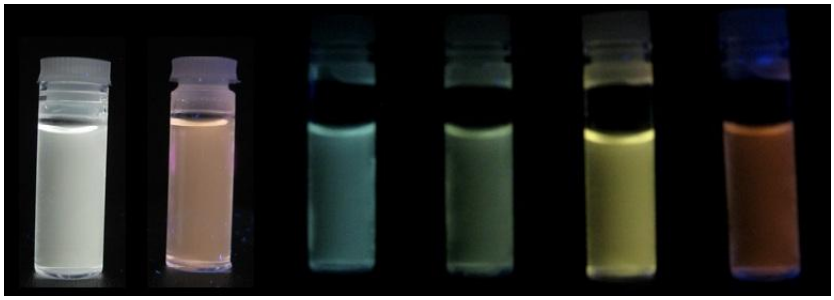

Figure 35. CDS09, CDS13, CDS19, CDS20, CDS23, CDS18 (from left to right)

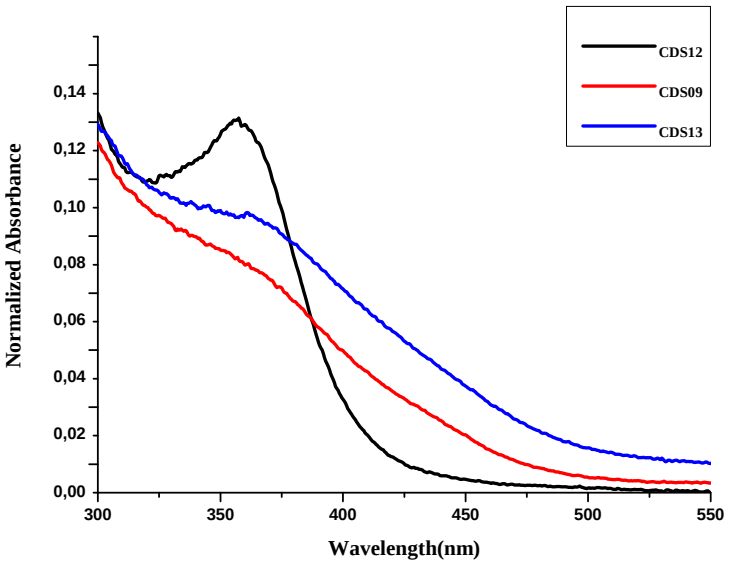

Figure 36 Uv-Visible absorbance spectra of CdS at a Ligand/Cd of 4, 2.5 and 1.5.

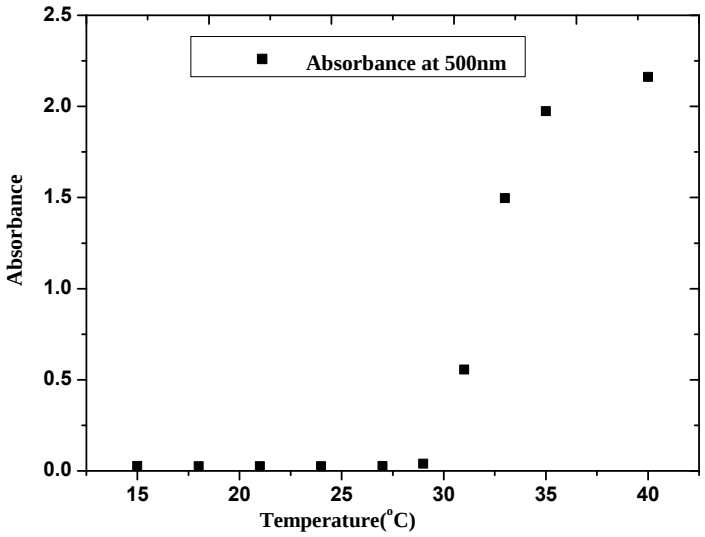

Figure 37. Absorbance readings plotted against temperature

As stated earlier, LCST of PDMAEMA is strongly dependent on the pH. Since at higher pH values, polymer will have a more hydrophobic character; LSCT that shows the cloud point arising from the aggregation of the polymer chains will be observed at lower temperatures. For the determination of LCST at pH 10, absorbance measurements of CDS12 were taken at 500 nm as a function of temperature (15-40 ºC) to evaluate the solution turbidity change associated with LCST. The cloud point was observed at around 30 ºC (Figure 37). Due to the instrumental limitations, we could not perform the experiment at lower pH values.

Hydrodynamic size of the particles should be influenced by the hydration of the shell, temperature and the pH. Therefore, sizes of the particles were measured by DLS at pH values 7,5 and 8,3 and at 25° and 60°C. In both cases hydrodynamic size decreased dramatically with increasing temperature, due to responsiveness of PDMAEMA used as coating material of quantum dots, as seen in figures 38 & 39. At the collapsed or more appropriate to say semi-collapsed phase, PDMAEMA could create a physical limitation for the growth of crystals as well. So, at smaller micellar reactors created by the polymer, smaller particles were formed. This helps to understand the results of reactions CDS19 and CDS21: CDS19 synthesized at 60 ºC

show luminescence in **blue**, whereas CDS21 synthesized at room temperature show luminescence in **green**, indicating formation of larger particles at lower temperatures Also at the same temperature as the pH increased from 7.5 to 8.3 size has decreased from about 400 to 300 nm indicating more compact structure. From the reactions CDS19 and CDS 20, it is understood that size decreases as the pH increases

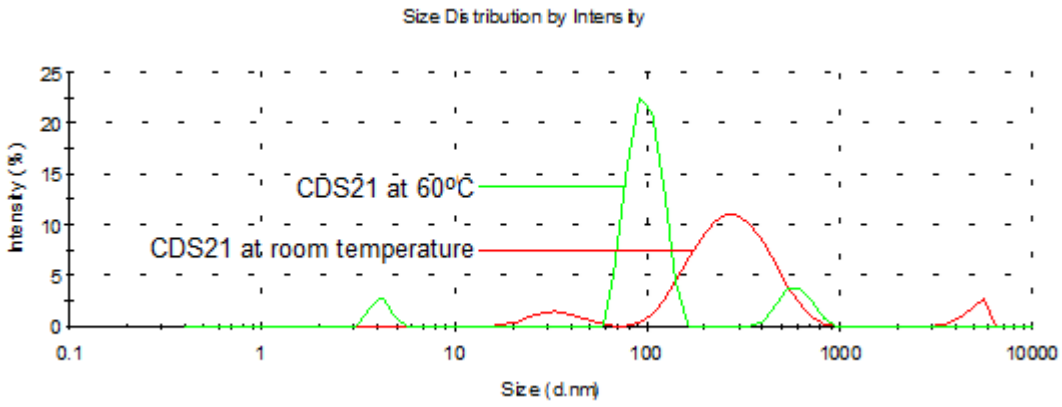

Figure 38. Hydrodynamic sizes of PDMAEMA/CdS (CDS21) at of the pH 8.3measured by DLS

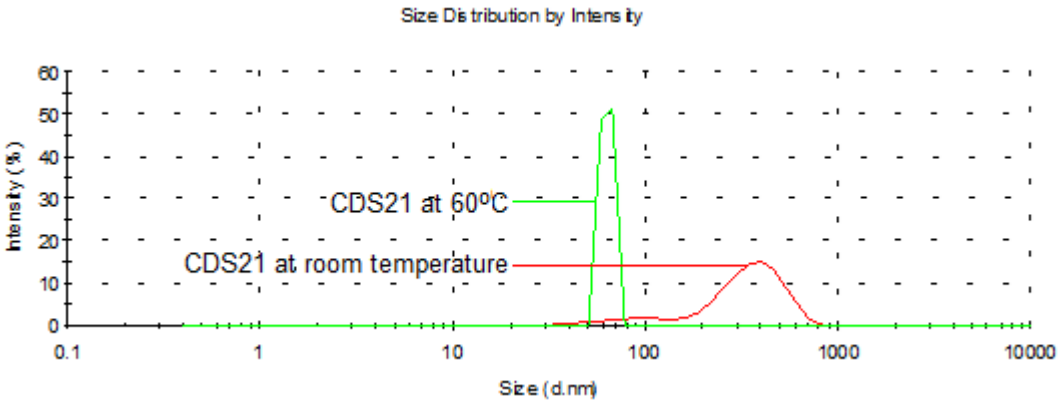

Figure 39. Hydrodynamic sizes of PDMAEMA/CdS (CDS21) at of the pH 7.5 measured by DLS

Hydrodynamic sizes were measured in a wider temperature range at pH 8,3 as well, as seen in Figure 40. As expected, due to the shrinkage of thermosensitive polymer chains bound to the crystal surface, shell (coating) thickness decreases, causing a

decrease in the hydrodynamic size from 120 nm to 48 nm with the increasing temperature up till 80°C. However beyond this point, hydrophobic nature and the coagulation of collapsed polymer chains causes particle aggregation causing an increase in the size, which would eventually cause precipitation at higher temperatures.

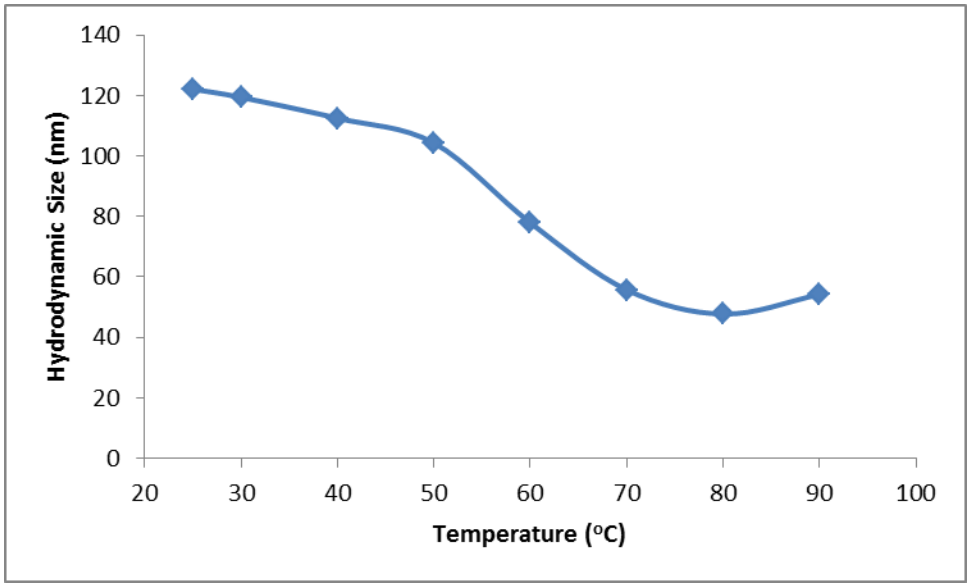

Figure 40 Change in the hydrodynamic size of aqueous PDMAEMA coated CdS21 with temperature. Reported values are averages of the intensity (or number) based averages calculated by DLS

Influence of the temperature and the related phase change on the luminescent properties of PDMAEMA/CdS was investigated through luminescence measurements. PL spectra of the samples (at neutral pH) were taken at different temperatures. As seen in Figure 41 photoluminescence intensity decreases dramatically with increasing temperature. DLS measurements indicated collapse of the polymer and aggregation with increasing temperature. Such aggregation would cause concentration quenching which will be reflected as a drop in the luminescence intensity. Increasing temperature could influence the coupling of the charge carries as well, which should be studied independently. Moreover, PL measurements demonstrate a valuable behavior: Drop in the luminescence is reversible! Photoluminescence intensity decreased about 52% as the temperature increased from

25 to 80°C. However, it reaches approximately to the initial value when the sample was cooled back to room temperature. Another interesting observation is ca 38nm red shift in the PL max as temperature was increased to 80°C, disappears when the sample was cooled back to the room temperature (Table 16).

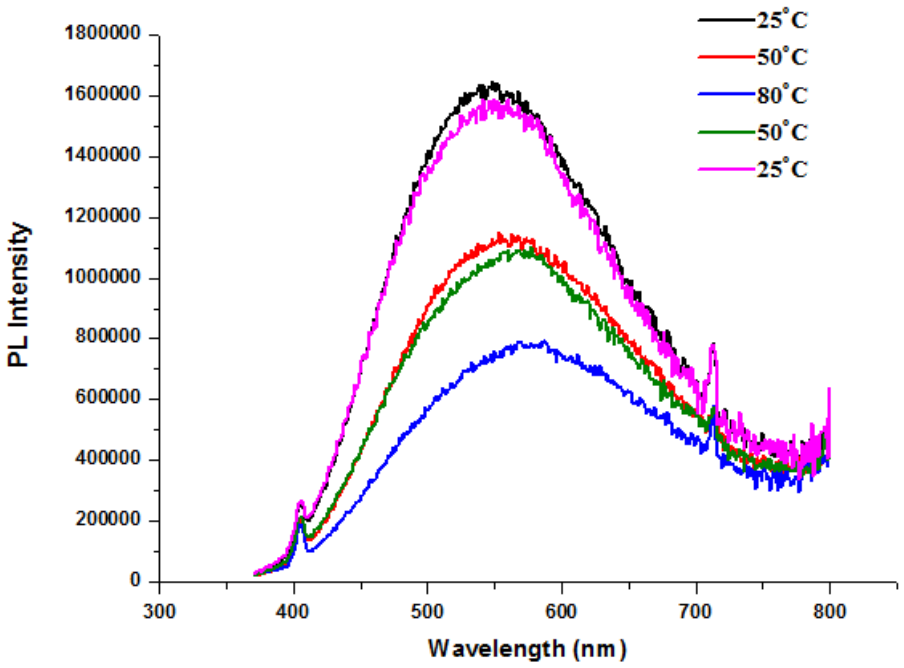

Figure 41. Comparison of PL intensity of CdS21 for diffferent temperatures, at pH 8.3

Table 16. Comparison of PL intensity of CdS21 nanoparticles at different temperatures, at pH 8.3

Temperature (°C)	Peak max (nm)	Intensity
25	**549**	**1,64E+06**
50	**553**	**1,15E+06**
80	**587**	**7,95E+05**
50	**577**	**1,10E+06**
25	**550**	**1,59E+06**

4.5 Conclusion

In this study, stable aqueous PDMAEMA CdS quantum dots in luminescing in different colors from blue to orange were synthesized through in situ coating approach. PDMAEMA itself was used directly as coating material in the synthesis of nanocrystals. In other words, PDMAEMA functions as a multidentate ligand thanks to its tertiary amine groups and nanocrytals can be synthesized in an easy, mild, one step process eliminating the complications and time consuming synthesis route of other approaches. Influence of reaction variables on the colloidal stability and luminescence properties were studied. Consequently, it was observed that, higher reaction temperatures, yet below the LCST of PDMAEMA, results smaller particles with higher quantum yield, since at higher temperatures PDMAEMA has smaller micellar size. Since PDMAEMA is both pH and temperature sensitive, its LCST is pH dependent. At lower pH values LCST of PDMAEMA increases due to the increase in the hydrophilicity of polymer (protonation of the amine groups) in acidic media. Since binding sites to cadmium are the amines of PDMAEMA, their protonation eliminates cadmium coordination and binding, rendering this polymer as an ineffective coating. Our results show that higher pH values usually causes a more compact structure and smaller QDs with higher QY. Effects of PDMAEMA amount and molecular weight on the nanocrystal size are also investigated. Employing PDMAEMA with lower molecular weight, resulted in smaller particles with lower quantum yield. Increase in the ligand amount produces smaller particles with higher quantum yield. Therefore, shorted chains in larger amounts are more effective in passivating the surface of the QD during the synthesis to control particle growth more efficiently.

Another advantageous feature of this approach is the possibility of the synthesis of PDMAEMA coated CdS nanoparticles both in water and in organic solvents such as DMF. However, the most striking feature of these materials is the combination of photoluminescence of quantum dots with the pH/temperature responsiveness of PDMAEMA. QDs that are responsive to pH and temperature are highly desirable for

biological applications and sensors. Besides, reversibility of the changes as a response to such stimuli makes these QDs great candidates for such applications.

In conclusion, these stimuli responsive quantum dots, thanks to their superior properties and easy processibility, have proven to be one of the most promising smart materials in this field.

Chapter 5 Smart Hybrid Nanoparticles

5.1 Introduction

In this study, for the first time in literature, we have developed a completely novel route for the synthesis of "smart" magnetic/luminescent hybrid nanomaterials.

As discussed previously, both magnetic and fluorescent nanoparticles have great scientific and technological importance. The combination of a magnetic and a fluorescent entity may provide a new two-in-one multifunctional nanomaterial with a broad range of potential applications such as multiplexing, dual imaging, dual action of sensing and separation or imaging and therapy.

There are several different methods employed for the synthesis of QD/MNP hybrids. In the first method QDs and MNPs were simultaneously embedded into a silica nanosphere via reverse microemulsion [106]. However, the distances of QDs and MNPs usually were too close to be controlled, leading to a strong interaction between QDs and MNPs, which may diminish the photoluminescence (PL) dramatically. Actually, there have been several studies devoted to the development of magnetic/fluorescence hybrids, but these materials suffer from the fluorescence quenching since iron oxide absorbs the photons emitted by the QDs in the visible range [106-107]. Until now no satisfactory solution to this problem has been proposed.

In the second method, hybrid nanoparticles were constructed by the layer-by-layer self-assembly technique [108]. This method allows the spatial separation of the magnetic domains from the fluorescent ones. As an example, magnetically modified polystyrene capsules have been used as templates on which negatively charged CdTe quantum dots were entrapped by means of a positively charged polyelectrolyte polymer. However, separations between the two particles are not large and in addition the process is quite tedious.

Our strategy proposes a universal and systematic approach for minimizing the quenching problem. This involves growth of an amphiphilic block copolymer from

the surface of one type of nanoparticle (MNP or QD) through ATRP. Immediate polymer block should have an appropriate chemistry to separate the MNPs from QDs, so, it should not interact with either polymer. The second or the outer block should stabilize the second type of nanoparticle (MNP or QD). In this thesis work, polymerizations were started from the surface of iron oxide and then QDs were synthesized within the outer block. The final structure was MNP-poly(styrene)-b-poly(dimethylamino ethyl methacrylate)/QD. There are few advantages of this strategy: the ability to control the chain length since ATRP is a controlled polymerization method. This would allow to adjust the separation between MNPs and QDs and to determine the optimum separation. Such information would lead the way to highly luminescent QD/MNP hybrids. Since molecular weights can be controlled, the second block which will act as a coating for the QD can be prepared at different molecular weights. This would provide means to alter and optimize QD properties. Besides, since ATRP is compatible with many monomers, the intermediate block (in between the two particles) can be synthesized as a stimuli responsive polymer. This would allow a mechanism to bring particles together as a response to a stimuli which can be used as a sensing mechanism.

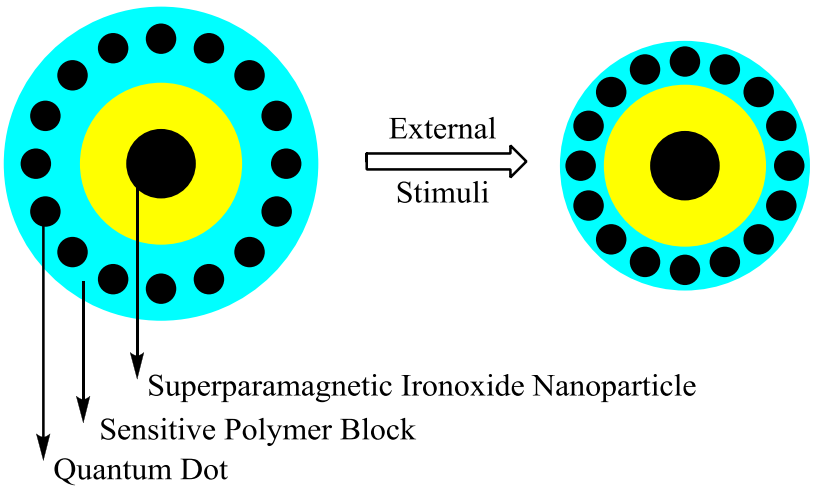

Figure 36. Schematic representation of smart hybrid nanoparticles

Alternatively, outer block which is responsible from coating the QD can be stimuli responsive as well. As stated earlier in this study, PNIPA, PHEMA and PEG failed to stabilize CdS QDs. On the other hand, CdS nanoparticles can be synthesized with a

PDMAEMA coat successfully. Therefore, the synthesis of stimuli responsive QD/MNP hybrids was achieved using PS-PDMAEMA coated MNP as a ligand in the CdS synthesis. However, it's important to note that this strategy is not limited to MNP and CdS quantum dots but it's a universal approach applicable to different nanoparticles.

5.2 Experimental

5.2.1 Materials

All chemicals were analytical grade or of the highest purity available. Sodium sulfide trihydrate ($Na_2S.3H_2O$), cadmium acetatedihydrate ($Cd(Ac)_2{\cdot}2H_2O$), Rhodamine B and HNO_3 (65 %) were purchased from Merck. Sodium hydroxide was purchased from Aldrich.

5.2.2 Synthesis of QD/MNP Hybrid

The synthesis follows a typical CdS synthesis procedure. The only difference from the PDMAEMA coated CdS synthesis procedure described earlier, is the ligand type and the solvent. PDMAEMA06, that is a MNP-PS_{1300}-b-$PDMAEMA_{290}$ (synthesis details given in Chapter 3), was used directly in the synthesis of CdS quantum dots. In a typical synthesis, 66,63 mg ($2{,}5.10^{-4}$ mol) $Cd(Ac)_2{\cdot}2H_2O$ was dissolved in 50 ml DMF and added to 250ml three-necked round bottomed flask fitted with a mechanical stirrer. 900 mg MNP- PS_{1300}-b-$PDMAEMA_{290}$ was added into the reaction flask. This solution was deoxygenated for 15 minutes, and brought in an oil bath at 60°C.

13.2 mg $Na_2S{\cdot}3H_2O$ was dissolved in 50 ml DMF/water in an ultrasonic bath and transferred into an addition funnel and deoxygenated for 15 min.

Sodium sulfide solution was added to the cadmium acetate solution drop by drop under nitrogen. After the addition was completed, reactants were stirred under nitrogen at set temperature for an additional hour. No further pH adjustment was done before UV-Vis or PL measurements.

Table 17. **Reaction Ratios of MNP/QD hybrid**

Ligand Type	Ligand/Cd	Cd/S	pH	T	Solvent
PDMAEM06*	**6**	**2,5**	**7,5**	**60**	**DMF/water**

* PDMAEM06 : MNP-PS_{1300}-b-$PDMAEMA_{290}$

5.2.3 Results and Discussion

One example to MNP-PS-block-PDMAEMA/CdS was successfully synthesized. This provides a solid proof for the concept. Yellow/orange luminescing hybrid nanoparticles are shown in Figure 43. Original yellow color of the sample originate from the iron oxide mostly.

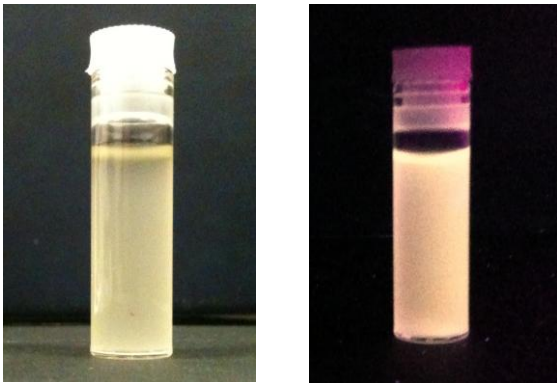

(a) (b)

Figure 37. Luminescent hybrid nanoparticle in daylight (a) and under UV excitation at 365 nm (b)

The UV-Vis and PL spectra are shown in Figure 44. UV-Vis spectrum shows a blue shift from the absorbance onset of CdS (512nm) indicating formation of QD. PL spectrum shows a maximum intensity at 590 nm.

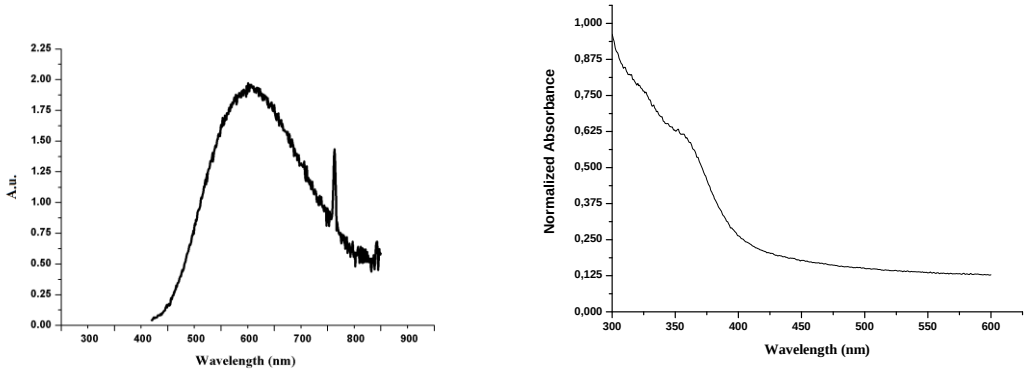

Figure 38. Absorbance calibrated PL spectra of MQD (left) UV-Visible absorbance sprectrum (right)

PDMAEMA (Mw=57K) coated CdS QDs which were synthesized in water at identical ligand/Cd (=6), Cd/S (=2.5) and temperature (60 ºC) were luminescing also yellow (CDS23 in Chapter 4). So, although the block length is slightly shorter (Mw=41K) and the reaction was done in water/DMF mixture, MNP-PS-block-PDMAEMA provided similar size QDs.

Actually, no discernible side effect was seen in the particle properties when CdS was synthesized in DMF as discussed in Chapter 4.

A major difficulty is the QY calculation of MQD. Since iron oxide nanoparticles absorb the excitation radiation at 355 nm, the fluorescence emission decreases significantly. Actually these particles emit around 600 nm and MNP should absorb that range! This is the second reason why QY calculation is not a reflection of QD quality. In other words, QY calculations for MQDs can't be performed accurately with current method. Iron concentration has to be determined and fluorescence intensity should be calibrated with respect to the iron concentration determined by the ICP.

The successful synthesis of MNP/QD hybrid nanoparticles is confirmed by UV/PL measurements. Therefore the procedure is shown to be viable for the production of hybrid nanoparticles.

5.3 Conclusion

In this chapter, we discussed the synthesis of MNP-PS-b-PDMAEM coated CdS nanoparticles as a first in the literature. This synthesis also provides a proof of concept for the novel approach proposed in this study. Further characterization of the product is necessary but the existing analysis proves the composition and the success in the synthesis.

A future study should focus on the synthesis of MQDs with different spacer length, as it would provide detailed information on the effect of MNPs on the luminescence performance of MQDs and allow determination of the optimum separation for the best luminescence properties. Furthermore, the modification of the chain length of PDMAEMA block should also be investigated, since this would impact the QD quality as described in Chapter 4.

Although, a single example is provided for the hybrid system, the approach was proven to be effective.

So next, in order to understand the importance of the separation between the two particles on the luminescent properties of the hybrids, the PS block length should be altered. This will lead the following efforts to the solution of the quenching problem in these hybrid compositions that awaits a solution. Further studies should also focus on the development of different blocks for QD stabilization. As proposed at the introduction, the final step would have been replacing PS block with a stimuli responsive block such as poly(N-isopropyl acrylamide) which will not have an interaction with MNP or QD but would provide a temperature response.

Chapter 6 CONCLUSION

Primary focus of this thesis was the development of smart CdS-MNP hybrid structures connected with polymer bridges. For this purpose, PDMAEMA coated CdS nanoparticles and surface initiated block copolymerization from MNPs were investigated in detail.

First, MNP surfaces were functionalized with a tertiary bromide and a primary chloride terminated alkoxysilane ligand by two different approaches, namely ligand exchange and one pot synthesis in DMF. Due to batch to batch differences encountered in direct synthesis in DMF, ligand exchange method was preferred to functionalize MNPs that will serve as ATRP initiator.

PMMA, PS, PS-b-PHEMA and PS-b-PDMAEMA were grown from the surface of iron oxide nanoparticles by using ATRP method. Most of the PMMA trials have undergone rapid gelation, which might be attributed to low initiator efficiency. For styrene polymerization, experiments under different reaction conditions were performed in order to obtain better control over the polymerization.

Based on our results, both CuII and free initiator addition led to relatively better control. However, due to its easier purification step, CuII addition was preferable since there was no noticeable difference in control between two approaches. Moreover, using CuCl as catalyst resulted in improved control compared to using CuBr. Yet, all trials resulted in polydispersity values higher than those expected for controlled polymerization. High polydispersities, together with the molecular weights that are higher than theoretical values point to low initiator efficiency as reported also in the literature. Nevertheless, the polymer chain ends were still retaining living character and in order to obtain the targeted hybrid structures, PS-b-PHEMA and PS-b-PDMAEMA block copolymerizations were performed using MNP-PS as macroinitiator; disregarding apparently low control.

In PS-b-PHEMA case, GPC measurements couldn’t be performed due to low solubility of samples in THF because of increasing hydrophilic character originating

from growing PHEMA block. In PS-b-PDMAEMA case, different ligand/catalyst systems were tried. Most promising/successful combination turned out to be bipyridine/CuBR/o-DCB. The block polymer formation was supported by TGA, DLS and GPC measurements.

In the second part, the first in-depth study of PDMAEMA-CdS nanoparticles was performed, revealing important and surprising characteristics of the system: CdS nanoparticles can be easily stabilized by PDMAEMA through tertiary amine end groups. The resulting hybrid materials are combining luminescence properties of CdS nanoparticles with reversible pH and temperature responsiveness of PDMAEMA.

Moreover, the size of the particles can be finely tuned by adjusting reaction parameters such as temperature, pH, ligand ratio and ligand molecular weight. Higher reaction temperatures, still below the LCST of PDMAEMA, resulted in smaller particles with higher quantum yield, as PDMAEMA has smaller micellar size at higher temperatures. In the context of pH parameter, while higher pH values usually cause a more compact structure and smaller QDs with higher QY, the reactions conducted at lower pH values terminates with bulk material. The reason behind this behavior is increased hydrophilicity of polymer (protonation of the amine groups) at lower pH values. Since binding sites to cadmium are the amines of PDMAEMA, their protonation eliminates cadmium coordination and binding, rendering this polymer ineffective for coating purposes.

There were interesting results concerning also the ligand effect on reaction control. Increase in the ligand amount produces smaller particles with higher quantum yield Employing PDMAEMA with lower molecular weight resulted in smaller particles with lower quantum yield. Therefore, shorted chains in larger amounts are more effective in inactivating the surface of the QD during the synthesis to control particle growth more efficiently.

Moreover, as a practical contribution to the literature, the synthesis of PDMAEMA coated CdS nanoparticles was performed both in water and in organic solvents such as DMF.

Finally, the synthesis of MNP-PS-b-PDMAEM coated CdS nanoparticles was achieved as a first in the literature. While only a single example is provided for this smart hybrid system, and characterizations are still ongoing, the approach was proven to be effective. Moreover, this approach opens the way for the efforts to solve the quenching problem in these hybrid compositions. Future work should focus on the synthesis of hybrids with different PS block lengths in order to understand the importance of the separation between the two particles on the luminescent properties of the hybrids.

In conclusion, this study not only provides the method for producing a multifunctional magnetic/luminescent nanostructure together with sensing mechanism, but also offers a novel approach to overcome the problems that set back the field for too many years.

References

[1] **Gogotsi, Y.,** 2006. Nanomaterials Handbook, CRC Taylor and Francis, Boca Ratón, FL.
[2] **Ozin, G. A., Arsenault, A, C.**, 2005. Nanochemistry: A chemical approach to nanomaterials, RSC Publishing, Cambridge, UK.
[3] **Rotello, V.**, 2004. Nanoparticles: building blocks for nanotechnology (Series: Nanostructure Science and Technology), Springer.
[4] **Kelly, K.L., Coronado, E., Zhao, L.L., G.C. Schatz,** 2003. J. Phys. Chem. B, **107**, 668.
[5] **Michalet, X.,** 2005. Science, **307**, 538.
[6] **Johnston, K. W., Pattantyus-Abraham, A. G., Clifford, J. P., Myrskog, S. H., Mac Neil, D. D., Levina, L., Sargent, E. H.,** 2008. Appl. Phys. Lett., **92**, 151115.
[7] **Schwertmann, U., Cornell, R. M.,** 1991. Iron oxides in the laboratory: preparation and characterization. Weinheim, Cambridge: VCH.
[8] **Kawashita, M., Tanaka, M., Kokubo, T., Yao, T., Hamada, S., Shinjo, T.,** 2002. Key Eng Mater, **218–220,** 645-648.
[9] **Roberts, M. J., Bentley, M. D., Harris, J. M.,** 2002. Adv Drug Del Rev, **54(4),** 459–76.
[10] **Sahoo, Y., Pizem, H., Fried, T., Golodnitsky, D., Burstein, L., Sukenik, C. N., Markovich, G.,** 2001. Langmuir, **17,** 7907–11.
[11] **Gupta, A. K., Gupta, M.,** 2005. Biomaterials, **26,** 3995-4021.
[12] **Alivisatos, A.P.,** 1996. Science, **271,** 933.
[13] **Advincula, R.,** 2001. Chemical Reviews, **101,** 9.
[14] **Pyun, J., Kowalewski, T., Matyjaszewski, K.,** 2003. Macromol. Rapid Commun., **24,** 1043–1059.
[15] http://www.qdots.com/new/technology/what.html
[16] CdSe Quantum Dots and Luminescent/Magnetic Particles For Biological Applications, **Thesis by Desheng Wang,** University of New Orleans, 2004.
[17] **Trindade, T., O'Brien, P., Pickett, N. L.**, 2001. Chem. Mater., **13**, 3843-3858.
[18] **Berry, C.R.**,1967. Phys. Rev., **161**, 848-851.
[19] **Brus, L.E.,** 1983. J. of Chem. Phys., **79 (11)**, 5566-5571.
[20] **Brus, L.E., Rossetti R., Ellison J.L., Gibson J.M.,** 1984. J. of Chem. Phys., **80 (9)**, 4464-4469.
[21] **Danek, M., Jensen, K. F., Murray, C. B., Bawendi, M. G.**, 1994. J. Cryst. Growth, **145**, 714.
[22] **Wang, Y., Herron, N.**, 1991. J. Phys. Chem., **95**, 525.
[23] **Li, X., Fryer, J. R., Cole-hamilton, D. J.**, 1994. Chem. Commun., **1994,** 1715.
[24] **Hagfeldt, A., Grätzel, M.**, 1995. Chem. Rev., **7**, 607.
[25] **Henglein, A., Gutierrez, M., Fisher, Ch. H. Ber. Bunsen-Ges.**, 1984. Phys. Chem., **88**, 170**.**
[26] **Nazzal, A. Y., Qu, L., Peng, X., Xiao, M.**, 2003. Nano Letters, **3(6)**, 819-822.
[27] **Kumar, K. N. P., Keizer, K., Burggraaf, A. J., Okubo, T., Nagamoto, H., Morooka, S.**, 1992. Nature, **48**, 358 .
[28] **Sberveglieri, G., Depero, L. E., Ferroni, M., Guidi, V., Martinelli, G., Nelli, P., Perego, C., Sangaletti, L.**, 1996. Adv. Mater., **8**, 334.
[29] **Chan, C. W., Nie, S.**, 1998. Science, **25**, 2016-2018.
[30] **Jaiswal, J. K., Simon, S. M.,** 2007. Methods Mol Biol., **374,** 93-104.
[31] **Goldman, E. R., Balighian, E. D., Mattoussi, H., Kuno, M. K., Mauro, J. M., Tran, P. T., Anderson, G. P.**, 2002. J. Am. Chem. Soc., **124(22),** 6378-6382.
[32]. **Han, M. Y.; Gao, X. H.; Su, J. Z.; Nie, S.**, 2001. Nature Biotech., **19(7)**, 631-635.

[33] **Parak, W., J., Pellegrino, T., Plank, C.**, 2005. Nanotechnology, **16**, R9-R25.
[34] **Kodama, R.H.,** 1999. Journal of Magnetism and Magnetic Materials, **200,** 359-372 .
[35] **Moghimi, S. M., Hunter, A.C. H., Murray, J. C.**, 2001. Pharm Rev, **53**, 283–318.
[36] **Curtis, A. S. G., Wilkinson, C**, 2001. Trends Biotech, **19**, 97–101.
[37] **Wilkinson, J. M.**, 2003. Med Device Technol., **14(5)**, 29–31.
[38] **Wang, Y. X., Hussain, S. M., Krestin, G. P.**, 2001. Eur. Radiol., **11**, 2319–2331.
[39] **Bonnemain, B.**, 1998. J Drug Target, **6**,167–174.
[40] **Nielsen, O. S., Horsman, M., Overgaard, J.**, 2001. Eur J Cancer, **37**, 1587–1589.
[41] **Scherer, F., Anton, M., Schillinger, U., Henke, J., Bergemann, C., Kruger, A., Gansbacher, B., Plank, C.**, 2002. Gene Ther., **9**, 102–9.
[42] **Hamley, I. W.**, 2003. Angew Chem Int Ed., **42**, 1692–1712.
[43] **Bai, Y., Teng, B., Chen, S., Chang, Y., Li, Z.**, 2006. Macromolecular Rapid Communications, **27**, 2107–2112.
[44] **Kim, B-S., Qiu, J-M., Wang, J-P., Taton, T. A.**, 2005. Nano Lett., **5 (10)**, 1987–1991.
[45] **Matyjaszewski, K.,** 1997. Am. Chem. Soc. Polym. Preprints, **38 (1),** 736-740.
[46] **Xia, J., Matyjaszevski, K.,** 1997. Macromolecules, **30,** 7697.
[47] **Odian, G.,** 1991. Principle Of Polymerization, 3rd Edition, Wiley, New York.
[48] **Greszta, D., Matyjaszevski, K.,** 1997. Am. Chem. Soc. Polym. Preprints, **38 (1),** 709.
[49] **Xia, J., Matyjaszevski, K.**, 2001. Am. Chem. Soc, **101**, 2921-2990.
[50] **Gupta A. K., Gupta M.**, 2005. Biomaterials, **26**, 3995–4021.
[51] **Bery, C. C., Wells, S., Charles, S., Curtis, A. S. G.**, 2003. Biomaterials, **24**, 4551–7.
[52] **Raghavarao, K. S. M. S., Doddamane, N., Sampangi Ch, Todd, P.W.**, 2002. Trends Biotechnol, **20**, 72–6.
[53] **Levy, L., Sahoo, Y., Kim, K. S., Bergey, E. J., Prasad, P. N.**, 2002. Chem Mater, **14**, 3715–21.
[54] **Kawashita, M., Tanaka, M., Kokubo, T., Yao, T., Hamada, S., Shinjo, T.**, 2002. Key Eng Mater, **218–220**, 645–8.
[55] **Sun, S., Anders, S., Hamann, H. F., Thiele, J-U., Baglin, J. E. E., Thomson, T., Fullerton, E. E., Murray, C. B., Terris, B.D.**, 2002. J Am Chem Soc, **124**, 2884–5.
[56] **Kondo, A., Fukuda, H.**, 1999. Colloids Surf A, **153**, 435–8.
[57] **Lowe, A. B., Sumerlin, B. S., Donovan, M. S., McCormick, C. L.**, 2002. J Am Chem Soc, **124**, 11562–3.
[58] **Ohno, K., Koh, K-m., Tsujii, Y., Fukuda, T.**, 2002. Macromolecules, **35**, 8989–93.
[59] **Li, D., He, Q., Cui, Y., Li, J.**, 2007. Chem. Mater., **19**, 412-417.
[60] **Hu, F., Neoh, K. G., Cen, L., Kang, T.**, 2006. Biomacromolecules, **7**, 809-816.
[61] **Zhou, Y., Wang, S., Ding, B., Yang, Z.**, 2008. Chemical Engineering Journal, **138**, 578–585.
[62] **Werne, T., Patent T. E.**, 2001. J. Am. Chem. Soc., **123**, 7497-7505.
[63] **Zhang, F., Xu, F. J., Kang, E. T., Neoh, K. G.**, 2006. Ind. Eng. Chem. Res., **45**, 3067-3073.
[64] **Tang, W., Matyjaszewski, K.**, 2007. Macromolecules, **40**, 1858-1863.
[65] **Hu, F., Neoh, K. G., Cen, L., Kang, E. T.**, 2006. Biomacromolecules, **7**, 809–16.
[66] **Wang, Y., Teng, X., Wang, J., Yang, H.**, 2003. Nano Letters, **3(6)**, 789–93.
[67] **Pluddemann, E. P.**, 1982. Silane coupling agents. Plenum Press, New York.
[68] **Shen, L., Stachowiak, A., Hatton, T.A., Laibinis, P.E** , 2000. Langmuir, **16**, 9907-9911.
[69] **Yagci Acar, H., Garaas, R. S., Syud, F., Bonitatebus, P., Kulkarni, A. M.**, 2005. J. Magnetism and Magnetic Materials, **29(1)**, 1-7.

[70] Selective Dispersion of Surface Modified Iron Oxide Nanoparticles in Polymer Blends, **Thesis by Özlem Tekmek**, Koç University, 2007.
[71] **Wu, N., Fu, L., Su, M., Asiam, M., Wong, K., Dravid, V. P.**, 2004. NanoLetters, **4(2)**, 383–6.
[72] **Hafeli, U., Schutt, W., Teller, J., Zborowski, M., Eds.**, 1997. Scientific and Clinical Applications of Magnetic Carriers, Plenum Press, New York.
[73] **Matyjaszewski, K., Gobelt, B., Paik, H.-J., Horwitz, C. P.,** 2001. Macromolecules, **34,** 430.
[74] **Kim, J. B., Huang, W. X., Miller, M. D., Baker, G. L., Bruening, M. L.,** 2003. J. Polym. Sci., Part A: Polym. Chem., **41**, 386.
[75] **Nanda, A. K., Matyjaszewski, K.,** 2003. Macromolecules, **36**, 599.
[76] **Nanda, A. K., Matyjaszewski, K.**, 2003. Macromolecules, **36**, 1487.
[77] **Pyun, J., Matyjaszewski, K.**, 2001. Chem. Mater., **13**, 3436.
[78] **Kamata, K., Xia, Y.,** 2003. J. Am. Chem. Soc., **125,** 2384.
[79] **Vestal, C. R., Zhang, Z. J.**, 2002. J. Am. Chem. Soc., **124,** 14312.
[80] **Wang, Y., Teng, X., Wang, J.-S., Yang, H.,** 2003. Nano Lett, **3**, 1008.
[81] **Liu, T., Jia, S., Kowalewski, T., Matyjaszewski, K., Casado-Portilla, R., Belmont, J.,** 2003. Langmuir, **19,** 6342–6345.
[82] **Ejaz, M., Yamamoto, S., Ohno, K., Tsujii, Y., Fukuda, T.,** 1998. Macromolecules, **31**, 5934.
[83] **Zhao, B., Brittain, W. J.,** 2000. Macromolecules, **33**, 8813.
[84] **Husseman, M., Malmström, E. E., McNamara, M., Mate, M., Mecerreyes, D., Benoit, D. G., Hedrick, J. L., Mansky, P., Huang, E., Russell, T. P., Hawker, C. J.,** 1999. Macromolecules, **32**, 1424.
[85] **Matyjaszewski, K., Miller, P. J., Shukla, N., Immaraporn, B., Gelman, A., Luokala, B. B., Siclovan, T. M., Kickelbick, G., Vallant, T., Hoffmann, H., Pakula, T.,** 1999. Macromolecules, **32,** 8716.
[86] **Jeyaprakash, J. D., Samuel, S., Dhamodharan, R., Rühe, J.**, 2002. Macromol. Rapid Commun., **23,** 277.
[87] **Matyjaszewski, K., Shipp, D., A., Wang, J-L., Grimaud, T., Patent, T., E.,** 1998. Macromolecules, **31,** 6836-6840.
[88] **Barbey, R., Lavanant, L., Paripovic, D., Schuwer, N., Sugnaux, C., Tugulu, S., Klok, H-A.,** 2009. Chem. Rev., **109,** 5437–5527.
[89] **Zammit, M. D., Davis, T. P., Haddleton, D. M., Suddaby, K. G.,** 1997. Macromolecules, **30,** 1915-1920.
[90] **Zhu, Y. J., Tan, Y. B., Du, X.,** 2008. eXPRESS Polymer Letters, **Vol. 2, No. 3,** 214–225.
[91]
[92] **Fogg, D. E., Radzilowski, L. H., Dabbousi, B. O., Schrock, R. R., Thomas, E. L., Bawendi, M. G.,** 1997. Macromolecules, **30,** 8433–8439.
[93] **Roth, P. J., Theato, P.,** 2008. Chem. Mater., **20,** 1614–1621.
[94] **Li, C., Han, J., Ryu, C. Y., Benicewicz, B. C.,** 2006. Macromolecules, **39,** 3175–3183.
[95] **Zhang, Q. L., Gupta, S., Emrick, T., Russell, T. P.,** 2006. J. Am. Chem. Soc., **128,** 3898-3899.
[96] **Zorn, M., Bae, W. K., Kwak, J., Lee, H. Lee, C., Zentel, R., Char, K.,** 2009. ACS, **5**, 1063–1068.
[97] **Dubois, F., Mahler, B., Dubertret, B., Doris, E., Mioskowski, C.,** 2007. J. Am. Chem. Soc., **129 (3),** 482–483.

[98] **Celebi, S., Erdamar, A. K., Sennaroglu, A., Kurt, A., Acar, H. Y.,** 2007. J. Phys. Chem. B, **111,** 12668-12675.
[99] **Wang, M., Felorzabihi, N., Guerin, G., Haley, J. C., Scholes, G. D., Winnik, M. A.,** 2007. Macromolecules, **40,** 6377-6384.
[100] **Duan, H., Kuang, M., Wang, D., Kurth, D. G., Angew, H. M.,** 2005. Chem. Int. Ed., **44,** 1717-1720.
[101] **Zhou, L., Gao, C., Xu, W.,** 2009. J. Mater. Chem., **19,** 5655–5664.
[102] **Dubois, F., Mahler, B., Dubertret, B., Doris, E., Mioskowski, C.,** 2007. J. AM. CHEM. SOC., **129,** 482-483.
[103] **Basua, S., Mondala, S., Chatterjeeb, U., Mandala, D.,** 2009. Materials Chemistry and Physics, **116,** 578–585.
[104] **Nair, A., Shen, J., Thevenot, P., Zou, L., Cai, T., Hu, Z., Tang, L.,** 2008. Nanotechnology, **19,** 485102.
[105] **Janczewski, D., Tomczak, N., Han, M-Y., Vancso, G. J.,** 2009. Macromolecules, **42,** 1801-1804.
[106] **Mandal, S. K., Lequeux, N., Rotenberg, B., Tramier, M., Fattaccioli, J., Bibette, J., Dubertret, B.,** 2005. Langmuir, **21,** 4175-4179.
[107] **Dubertret, B., Calame, M., Libchaber, A. J.,** 2001. Nat. Biotechnol., **29,** 365.
[108] **Zebli, B., Susha, A. S., Sukhorukov, G. B., Rogach, A. L., Parak, W. J.,** 2005. Langmuir, **vol. 21,** 4262-4265.